

Sun global Alfvén resonance from decade-scale dynamics of N–S separated fast solar wind

Mensur Omerbashich¹

¹Journal of Geophysics

November 21, 2022

Abstract

The Sun reveals itself in the 386–2.439-nHz (1-mo–13-yr) band of polar ($\varphi_{\text{sun}} > |70^\circ|$) fast ($> 700 \text{ km s}^{-1}$) solar wind's decade-scale dynamics as a globally completely vibrating/resonating magnetoalternator and not just a proverbial engine anymore. Thus North–South separation of hourly-averaged, 1994–2008 Ulysses samplings of the $< 10 \text{ nT}$ polar winds in $\sim 1.6 \cdot 10^7$ – $2.5 \cdot 10^9$ -erg energies revealed spectral signatures of a [?]99%-significant Sun-borne global differential resonant activity, verified across disparate data. Confirming the Alfvén's view on a Sun globally resonating under its $P_s \sim 11$ -yr Schwabe mode, this Alfvén (a-mode) resonance (AR) comprising Rossby-like r-modes and cavity-confined R-modes, is governed by P_s at a remarkable $\sim 25\%$ field variance northside, a ~ 9 -yr degeneration of P_s at $\sim 20\%$ southside, and a ~ 10 -yr degeneration of P_s under equatorial mixing. While composing the PG[?](88–100-yr) Gleissberg cycle, the 9–10–11-yr sector coupling also co-triggers AR, $P_i = P_s/i$, $i = 2 \dots n$, n [?], imprinted in the fast winds at least to the order $n = 100$. The overwhelming (anisotropy moderating) and deterministic (with $\Phi \gg 12$ fidelity) AR is accompanied by a most useful symmetrical antiresonance, $P(-)$, whose both N/S tailing harmonics $P(-)_{17}$ are the well-known 154-day Rieger period, from which the couplings-freed Rieger resonance sprouts as wind's own. Thus the Sun is a typical, ~ 3 -dB-attenuated ring system of differentially rotating and contrarily vibrating conveyor belts and layers, with a continuous spectrum of modes, patterns complete in both parities, and resolution better than 81.3 nHz (S) and 55.6 nHz (N) in lowermost frequencies ([?]2 μ Hz in most modes). Unlike a resonating car engine that tries but fails to separate its fixed casing, the resonating free Sun exhausts the wind in a shake-off alongside the rotational axis. AR advances standard stellar models, agrees with laboratory experiments for enhanced studies of the Sun interior and heliosphere, and can explain the million-degree corona and solar abundance.

Sun global Alfvén resonance from decade-scale dynamics of N–S separated fast solar wind

Mensur Omerbashich

<https://orcid.org/0000-0003-1823-4721>, editor@geophysicsjournal.com

Abstract. The Sun reveals itself in the 386–2.439-nHz (1-mo–13-yr) band of polar ($\phi_{\text{Sun}} > |70^\circ|$) fast ($>700 \text{ km s}^{-1}$) solar wind’s decade-scale dynamics as a globally completely vibrating/resonating magnetoalternator and not just a proverbial engine anymore. Thus North–South separation of hourly-averaged, 1994–2008 Ulysses samplings of the $<10 \text{ nT}$ polar winds in $\sim 1.6 \cdot 10^7 - 2.5 \cdot 10^9$ -erg energies revealed spectral signatures of a $\geq 99\%$ -significant Sun-borne global differential resonant activity, verified across disparate data. Confirming the Alfvén’s view on a Sun globally resonating under its $P_S \sim 11$ -yr Schwabe mode, this Alfvén (a-mode) resonance (AR) comprising Rossby-like r-modes and cavity-confined R-modes, ${}^a P = {}^r P \cup {}^R P$, is governed by P_S at a remarkable $\sim 25\%$ field variance northside, a ~ 9 -yr degeneration of P_S at $\sim 20\%$ southside, and a ~ 10 -yr degeneration of P_S under equatorial mixing. While composing the $P_G \in \sim (88-100\text{-yr})$ Gleissberg cycle, the 9–10–11-yr sector coupling also co-triggers AR, $P_i = P_S/i$, $i=2\dots n$, $n \in \aleph$, imprinted in the fast winds at least to the order $n=100$. The overwhelming (anisotropy moderating) and deterministic (with $\Phi \gg 12$ fidelity) AR is accompanied by a most useful symmetrical antiresonance, P' , whose both N/S tailing harmonics P'_{17} are the well-known 154-day Rieger period, from which the couplings-freed Rieger resonance sprouts as wind’s own. Thus the Sun is a typical, ~ 3 -dB-attenuated ring system of differentially rotating and contrarily vibrating conveyor belts and layers, with a continuous spectrum of modes, patterns complete in both parities, and resolution better than 81.3 nHz (S) and 55.6 nHz (N) in lowermost frequencies ($\lesssim 2 \mu\text{Hz}$ in most modes). Unlike a resonating car engine that tries but fails to separate its fixed casing, the resonating free Sun exhausts the wind in a shake-off alongside the rotational axis. AR advances standard stellar models, agrees with laboratory experiments for enhanced studies of the Sun interior and heliosphere, and can explain the million-degree corona and solar abundance.

Sun engine; Sun global Alfvén resonance; Sun a-mode vibration; solar wind; Rieger resonance; Rieger periodicities; standard stellar models; million-degree corona; solar abundance.

1. Introduction

The Sun is a magnetic star commonly believed to owe its magnetism to *dynamo* — a process occurring in the deep interior and in which kinetic energy (here of core motion, mostly primordial rotation) gets converted into electric energy that naturally gives rise to magnetic fields maintained then by turbulence and other complex motions (Solanki et al., 2006). The mechanism for solar magnetism could also be convectional due to plasma/gas flows (Route, 2016) and hemispherical due to Sun’s characteristic latitudinal variations (Grote and Busse, 2000). Indeed, one of the main results from Ulysses — the only Space mission that flew above the Sun’s polar ($\phi_{\text{Sun}} > |70^\circ|$) regions — has revealed latitudinal differentiation of our star’s magnetism, discovering significant variations in-between the poles as well as from that of the rest of the Sun, which is dominated equatorially in a “streamer belt” regime. Ulysses also made the first *in situ* observation of solar magnetic polarity reversals — occurring over several months of maximum (magnetic) activity of the Sun, or once every ~ 11 yr, which confirmed earlier such indications by the Wilcox Solar Observatory (WSO) (Jones and Balogh, 2003). This quasiperiodicity agrees with the average *Schwabe cycle*, $P_S \in [9 \text{ yr}, 13 \text{ yr}]$, commonly noted since its discovery as a quasi-periodic variation in the number of magnetism-absent (“dark”) surface regions — *sunspots* (Schwabe, 1844).

Given our star’s size and mass, it is reasonable to assume that this is no coincidence and that the Ulysses result is extendable to mean that the Sun behaves as a magnetic alternator engine, known to normally both vibrate and resonate, i.e., vibrate additionally after its fundamental mode of vibration matched that of another physical system or its subsystem. Namely, when due to physical coupling with a subsystem, the resonance is triggered internally (self-resonating system), and when it arises in decoupled systems and systems, externally, e.g., orbitally. The Father of the widely used magnetohydrodynamics (MHD) theory (Alfvén, 1942) held a view that the ~ 11 (~ 22)-yr must be the global resonance period of existing lines of force in the Sun interior (Alfvén, 1943). Thus the *Alfvén waves* are a type of compressional magneto-acoustic waves in the Sun (Campos, 1977), which propagate along magnetic lines of force with a velocity proportional to the magnetic field, and can become transverse or perpendicular to the wave motion

when they are called kinetic (Alfvén) waves, cf., Alfvén (1942, 1948). The concept of such *Alfvén resonance* (AR) has been opposed, e.g., by Bellan (1994), as well as defended, e.g., by Goedbloed and Lifschitz (1995). While Bellan (1996) found from theoretical considerations that AR is a feature of ideal MHD only, and therefore cannot arise in reality, Grant et al. (2018) deduced from observations of a sunspot that, under certain atmospheric conditions, magnetic field-lines flapping, i.e., the Alfvén waves, could form resonantly driven shocks and dissipate into thermal energy. Modeling by Srivastava et al. (2017) suggested that observed high-frequency ($\sim 12\text{--}42$ mHz) torsional oscillations in the quiet Sun are torsional Alfvén waves and that they transfer $\sim 10^3 \text{ W}\cdot\text{m}^{-2}$ energy into the overlying corona, sufficient to heat it and facilitate the creation of the solar wind. In addition, a linear scaling law has been observed independently from Ulysses mission data, spanning more than two decades and holding across a wide range of scales extending from few minutes up to 1-day and longer (inertial) scales (Sorriso-Valvo et al., 2007), indicating that the Sun drives solar-wind turbulence itself (Bruno and Carbone, 2013). The unexpected existence of the scaling law in anisotropic, weakly compressible, and inhomogeneous turbulence still needs to be fully understood (Sorriso-Valvo et al., 2007). This linear scaling is the first large-scale evidence that solar-wind turbulence could be describable using the MHD theory.

It is well established that the Sun and other stars are vibrating bodies (Deubner and Gough, 1984), whose vibrations, magnetism, polarity, and AC (current), propagate via released magnetized plasma (atmosphere's thermally ionized gas; mostly H^+ - He^{2+} charged particles). The released plasma is named *solar wind*, and it propagates into the heliosphere, where the wind's magnetization is then called the *interplanetary magnetic field* (IMF). The Sun's and heliosphere's vibrations occupy various ranges: 4–15-minute short-period and 2-hour–12-day intermediate long-period bands (Thomson et al., 1995), the $\sim 7\text{--}30$ -day long-period band dominated by the Sun's ~ 27 -day surface mean rotational phase (Choi and Lee, 2019), the ~ 30 -day–1-yr long-period band dominated by the widely reported $P_{\text{Rg}} = \sim 154$ -day Rieger period (Rieger et al., 1984) and its $\frac{5}{6}P_{\text{Rg}}$, $\frac{2}{3}P_{\text{Rg}}$, $\frac{1}{2}P_{\text{Rg}}$, $\frac{1}{3}P_{\text{Rg}}$, $\frac{1}{5}P_{\text{Rg}}$ harmonics, i.e., ~ 128 , ~ 102 , ~ 78 , ~ 51 , ~ 31 -days periods referred to as Rieger-type periodicities (Dimitropoulou et al., 2008), 1–2-yr intermediate very-long-period ranges (Forgacs-Dajka and Borkovits, 2007), as well as occasionally reported longer-period bands ranging from $\sim 1\text{--}11$ yr, e.g., Vecchio and Carbone (2009) and Deng et al. (2014).

The first known attempt at recovering the Sun global field-line resonance, as driven by P_{S} and first proposed by Alfvén (1943), was by Stenflo and Vogel (1986) and Knaack and Stenflo (2005), from the Sun data and using spherical harmonic decomposition modeling with Lomb-Scargle and wavelets spectral techniques. However, their result was dubious as built on inapt techniques applied to regions of deviating turbulence, e.g., Bruno and Carbone (2013), and represented by data of questionable quality so that their alleged recovery turned out to be sparse (in one alleged parity only and without any reasonably discernable patterns) and coarse (both inaccurate and imprecise). Also, there have been reports of solar-wind resonances but in shorter-period ranges and mostly centered on the Sun rotational frequency, e.g., by Singh and Badruddin (2019). One prominent case of a solar wind's global systematic dynamic is the *Rieger resonance* (RR), encompassing a train of the mentioned Rieger-type harmonics driven by P_{Rg} , and for which Bai and Cliver (1990) suggested could be simulated with a damped, periodically forced nonlinear oscillator that exhibits both periodic and chaotic behavior. Rieger-type periodicities could be explainable by Rossby-type waves or another effect (Knaack and Stenflo, 2005). RR was reported in the IMF, including Earth vicinity (Cane et al., 1998), and in different ranges depending on data, location, epoch, and methodology, as 155–160 days, 160–165 days, 175–188 days, and 180–190 days (Gurgenashvili et al., 2017). Thus while Rieger resonance occurs in various ranges, those share the 30–180-days band. Historically, the Rieger period has decreased until the middle of the last century and then began to increase again towards the end of the century, opposite to the activity magnitude trend (Zaqarashvili et al., 2010). Likewise, Rieger-type periodicities also correlate with solar cycle strength and are shorter during solar cycles with higher magnetic activity (Gurgenashvili et al., 2016). This situation implies that Rieger resonance originates in the Sun engine. However, possible upstream waves in the solar wind from termination shock on the order of a few days and longer were implied from Voyager 2 mission samplings of the solar wind on entry into the interstellar space, allowing for the classical explanation according to which a mechanical resonance can arise due to waves encountering physical obstacles along propagation paths.

Unlike spectra of spheroidal p- (pressure-force-; compression-restored-) and g-mode (gravity-force-; buoyancy-restored-) vibrations with >1 h periods and extracted often in the past, toroidal R-mode (cavity-confined; electromagnetic-force-restored-) resonances (Dzhalilov et al., 2002) and geometrical r-mode (Rossby-waves-like; Coriolis force-restored) months-long periods remain elusive and rarely tackled (Knaack and Stenflo, 2005). Crude estimates indicate that R-mode periods are in the range of years and inexplicable by dynamo theory (Stenflo and Vogel, 1986). Since the latter two types of long-periodic vibration occupy two adjacent portions of the subrotational frequencies (periods from ~ 30 -day to ~ 11 -yr), i.e., the entire band of interest in the present study, they herein are considered together and so conjointly termed the a-mode (globally-triggered-and-restored-) resonant vibrations or AR for Alfvén Resonance, with periods ${}^aP = {}^rP \cup {}^R P$. In stars with a uniform rotation, very-low subrotational frequency vibrations (like the a-mode vibration) are likely candidates for (global) resonance with the orbital motion (Papaloizou and Pringle, 1978), which due to our Sun’s non-uniform rotation excludes external triggering of global resonances. Furthermore, in cases of non-uniformly rotating stars like our Sun, we can expect to see a continuous spectrum of modes that can undergo amplification and hence lead to enhanced dissipation (*ibid.*).

Spacings and orientations of current sheets in the solar wind reveal that the magnetic structure of the heliosphere is a network of braided magnetic-flux tubes of unknown origin (Borovsky, 2018). These hypothetical tubes could arise as propagating modes experience resonances that generate coherent structures in the solar wind, allowing for the solar origin of the convected component of interplanetary MHD turbulence (Bruno and Carbone, 2013). Field-line resonance was invoked previously as the mechanism behind two still unresolved problems of large-scale dynamics: solar abundance (Asplund et al., 2009) and the million-degree corona (Davila, 1987). And while the internal heating of the solar wind on release is due to small-scale ion-cyclotron resonance (Kasper et al., 2013), global overheating of the corona and the peculiar intrinsic acceleration of the solar wind to distances of $\sim 10R_{\odot}$ or ~ 0.05 AU likely share the same (unknown) underlying mechanism (Grail et al., 1996). Completing global knowledge of the Sun would have very large implications for our understanding of stars and galaxies in general (Bergemann and Serenelli, 2014). For example, such a breakthrough would cast light on how stars lose mass and angular momentum to stellar winds, while r-modes, if measured, will become sensitive new probes of stellar physics and structure (Wolff and Blizard, 1986).

The present study then aims at extracting a signature of the Sun’s global periodic information as imprinted in the nearby solar wind using the apt methodology to analyze gapped data. Note the use of the term *vibrations* for dynamical and *oscillations* for kinematical (“without mass”) macroscopic considerations. Namely, when speaking of vibrations, one is prompted to think in terms of dynamics, i.e., mechanical waves physically discernable as they propagate through (all forms of) matter, which is most useful for practical considerations. Referring to oscillations requires mostly abstract thinking, primarily in terms of kinematics (like orbital), but also in terms of other geometric relations, and it is useful primarily for theoretical considerations.

2. Data and methodology

To extract the Sun periodicities in the band of magnetic polarity flipping, I compute spectra of the only type of globally emitted solar wind whose origin is undisputed - the fast (>700 km·s $^{-1}$) wind, emitted mainly from polar regions; sources of the slow wind (~ 400 km·s $^{-1}$) and their locations remain a matter of debate (Brooks et al., 2015). Thus I regard the fast wind as ideal, i.e., matching the original physical conditions for the release as closely as possible. The goal is to put the often-heard syntagm on the *Sun internal engine* to a test by examining if how the Sun emits the wind corresponds in any way to a shake-off typical of many engines trying to rid themselves of their casing while experiencing a mechanical resonance. The resonance in such cases is due to irregularities in the engine structure and conditions or other factors that introduce jolts into vibration. Here I tacitly assume that variations in the Sun’s internal structure and composition can produce such mechanical resonances and that the (equatorially dominated) rest of the Sun mainly hosts sources of the slow wind.

I carry the examination first in the little-explored portion of $<\sim 11$ -yr solar vibrations: the 1–13-yr very-long-period (31.71–2.439-nHz) range of the flipping itself, or in the ~ 0.01 – 0.13 -ZeV ($\sim 1.6 \cdot 10^7$ – $2 \cdot 10^8$ erg) band of solar-wind extreme energies. Namely, if a systematic physical process could be identified spectrally within the highest system energies, contrary to smooth spectra due to turbulence, then the process is most likely caused by the Sun’s internal engine (Gough, 1995). Furthermore, if the mechanism can be shown resonant in the band of interest, as established previously for other bands, then the Sun demonstrably behaves like and maintains the state of a magnetic alternator engine. Then as such, the Sun can be expected to resonate predictably, which is usable for probing the interior based on a simple premise of physical sciences — that on a most general utility of any regular propagation of energetic waves that are within reach of our instruments.

Secondly, I investigate if the heliosphere maintains solar a-mode vibrations, as transpired via the solar wind, in the band of interest. If so, that would allow learning more about the inner workings of the Sun and the energy budgets of the heliosphere (Brooks et al., 2015). Successful extraction of vibration information here could allow learning from modal analysis of resonances (Deubner and Gough, 1984) and to the degree that depends upon the regularity and strength of a resonant process. In addition, any detection of a-modes would provide a substantial new probe of the Sun interior rotation and, eventually, a constraint on convection theory (Wolff and Blizard, 1986). Note here that Fossat et al. (2017) have meanwhile claimed the absolute value for the Sun core rotation of \sim one week. To achieve the goal and extract the desired information in an approach modernized both in terms of data and methodology, I use the four of, for global studies arguably the best, data sets of solar and solar wind’s magnetic fields data. Thus to examine how well the heliosphere maintains wind vibrations, I compare the spectra of the Sun global fields (mean magnetic field (MMF) and polar fields (PF) from the WSO telescope (Scherrer et al., 1977), and polar magnetic fields as reflected in the fast wind from Ulysses) against the spectra of IMF at L1 from WIND mission. Here MMF is presumed dominated by background/equatorial fields in a $\sim 9:1$ ratio to other magnetic features, including local fields, i.e., sunspots (Bose and Nagaraju, 2018), and reflected in the slow wind. Since here the MMF and WIND data are taken to depict relatively slow vs. fast wind at its sources, respectfully, their matching of the L1 dataset would mean that the heliosphere reflects solar vibrations in the band of interest at planetary distances.

As mentioned earlier and based on previous studies of Ulysses measurements, while the Sun emits the fast wind from polar regions, the slow wind emitted from lower heliographic latitudes gets slowed down by rotation and thereby equatorially mixed to the streamer belt regime; see, e.g., Smith and Marsden (2003). Then from the perspective of the Sun vibrating like a classical magnetically alternating motor as well, the fast (polar) wind should reflect the Sun’s inner workings more faithfully than the slow (equatorially mixed) wind ever could. Importantly, since the polar regions themselves emit the solar wind at significantly varying rates given the southern region’s instability due to higher turbulence and wandering fields, resulting in significant N–S asymmetry of solar wind speeds irrespectively of solar activity (Tokumaru et al., 2015), I also separate the polar data into northern and southern fast solar winds. Finally, if the fast solar wind indeed permeates the heliosphere in the band of polarity flipping, the Sun then should be expelling the wind at those same resonance modes too. In summary, after the separation of resonance from heliophysical background noise, the Sun structure, composition, and engine parameters could all be tackled from a new perspective based on modal analyses. This new perspective could enable gaining a more detailed if not complete insight into our star than previously attainable from using tools such as helioseismology, spectroscopy, cosmochemistry, or gravity modes. Finally, such new fundamental knowledge on the Sun’s inner workings would also improve our understanding of stars and star systems. Data used in the present study are depicted in Fig. 1. The spectral resolution is 1000 points/lines throughout the present study.

To compute spectra, I use the rigorous Gauss–Vaniček (GV) method of spectral analysis (GVSA) by Vaniček (1969, 1971), which represents spectral peaks against linear background noise levels. The spectral peaks can be expressed in percentages of the respective peak’s contribution to data variance (var%), as well as in decibels, dB (Pagiatakis, 1999). GVSA comes integrated with a complete statistical analysis into a scientific software package LSSA that provides periodicity estimates in the strictly least-squares sense, unlike the more popular Lomb-Scargle approximation that underperforms when analyzing noisy and complicated signals such as those of solar activity (Carbonell et al., 1992; Danilović et al., 2005). Tests of GVSA, showing its superiority, have been performed, e.g., by Taylor and Hamilton (1972) and

Omerbashich (2003). Using GVSA has many benefits and outperforms Fourier methods in numerous ways and situations; for example, when analyzing long gapped records, i.e., most records of natural data (Omerbashich, 2021a, 2007, 2006; Press et al., 2007; Pagiatakis, 1999; Wells et al., 1985). By discarding unreliable data in the record, such as non-calibrated telescope observations, I also take advantage of the blindness to data gaps as a feature exclusive to the least-squares class of spectral analysis techniques. This property of GVSA becomes a crucial advantage in analyses of scarcely clustering intermittent observations, like those of the solar wind above polar regions, which are intermittent because of the Ulysses mission objective to target polar regions as rarely observed, Fig. 1–c. The minimum number of values GVSA can estimate a spectrum from is three.

GVSA is rigorous because it both estimates a statistical significance in var% for the desired level, say 95%, in a spectrum from a time series with p data values and q known constituents as $1-0.95^{2/(p-q^2)}$ (Steeves, 1981) (Wells et al., 1985) and imposes the fidelity or “realism” (Φ) additional constraint to determine the validity on each significant spectral peak individually. As known from advanced statistics, fidelity is a general information measure based on the coordinate-independent cumulative distribution and critical yet previously neglected symmetry considerations (Kinkhabwala, 2013). In communications theory, fidelity measures how undesirable it is (according to some fidelity criterion we devise) to receive one information as another piece of information is transmitted (Shannon, 1948). Fidelity is then defined in GVSA, i.e., in the theory of spectral analysis, as a measure of how undesirable it is for two frequencies to overlap at (occupy) the same frequency space of a sample. A fidelity value then is that time interval (in units of the timescale) by which the period of a significant spectral peak must be elongated or shortened to be π -phase-shiftable within the time-series length. Φ then measures the unresolvedness between two consecutive significant spectral peaks (that cannot be π -phase-shifted). Two adjacent peaks are resolvable if their periods differ by more than the fidelity value of the former. This clustering tendency criterion reveals whether a spectral peak can share a systematic nature with another spectral peak, e.g., be part of a batch, an underlying dynamical process like resonance, antiresonance, reflection, overtone, undertone, etc. The spectral peaks that meet this criterion are in the LSSA software output listed amongst insignificant, and the rest amongst significant (hereafter: *physically-statistically significant peaks* or just (fully) *significant peaks* for short). Subsequently, Omerbashich (2006) deduced empirically an additional criterion of stringency: that GVSA fidelity in prominently periodic time series (with more than just a few periodicities) to reasonable approximation satisfies a $\Phi > 12$ common criterion for the individually genuine significance of a systematic process and therefore most of its periodicities as well.

To prevent aliasing, the band's lower end, 13-yr, was selected as not too close to P_s and as out of phase with the Ulysses orbital period, of 6.2 yr. Thanks to the ability of GVSA to handle spectral/energy leakages methodologically, i.e., simply by slightly adjusting the band limits if needed, this band choice should also prevent any leakages for that band. Also, unlike in the Fourier class of spectral analysis methods, GVSA does not depend on the Nyquist frequency, and so can fit trigonometric functions even in, i.e., extract significant periodicity from, data spanning intervals slightly (empirically: up to ~50%) shorter than twice the period of interest.

3. Results

Spectra of the data from Fig. 1 were computed first in the little-explored 1–13-yr (31.710–2.439-nHz or 100.00–7.69-cycles per century) band or the $\sim 1.6 \cdot 10^7 - 2 \cdot 10^8$ erg band of solar-wind extreme energies and plotted in Fig. 2 in five panels, respectively to the panels of Fig. 1 whose panel c also corresponds to Fig. 2–d & e after data separation into the southern and northern polar wind, respectively. As seen, notable spectra-wide features in the revealed series of ordered frequency response functions are resonance (sharp peaks) and to it symmetrical antiresonance (sharp troughs) trains, a ~3-dB attenuation typical of controlled mechanically resonating structures like engines (Ewins, 1995), and a constantly high relative system energy in the lead mode and all the harmonics, of ~25 var%. These features are typical of a classical motor and reflect the previously little understood workings of the often invoked Sun internal engine. The extracted solar-wind signature of a very-long-period resonance of solar magnetic fields contains several additional fundamental properties of vibrating/resonating systems, which are addressed in terms of this result's experimental validation later on. One property worth noting right away is the symmetry between the resonance and antiresonance, which reveals a real engine at work.

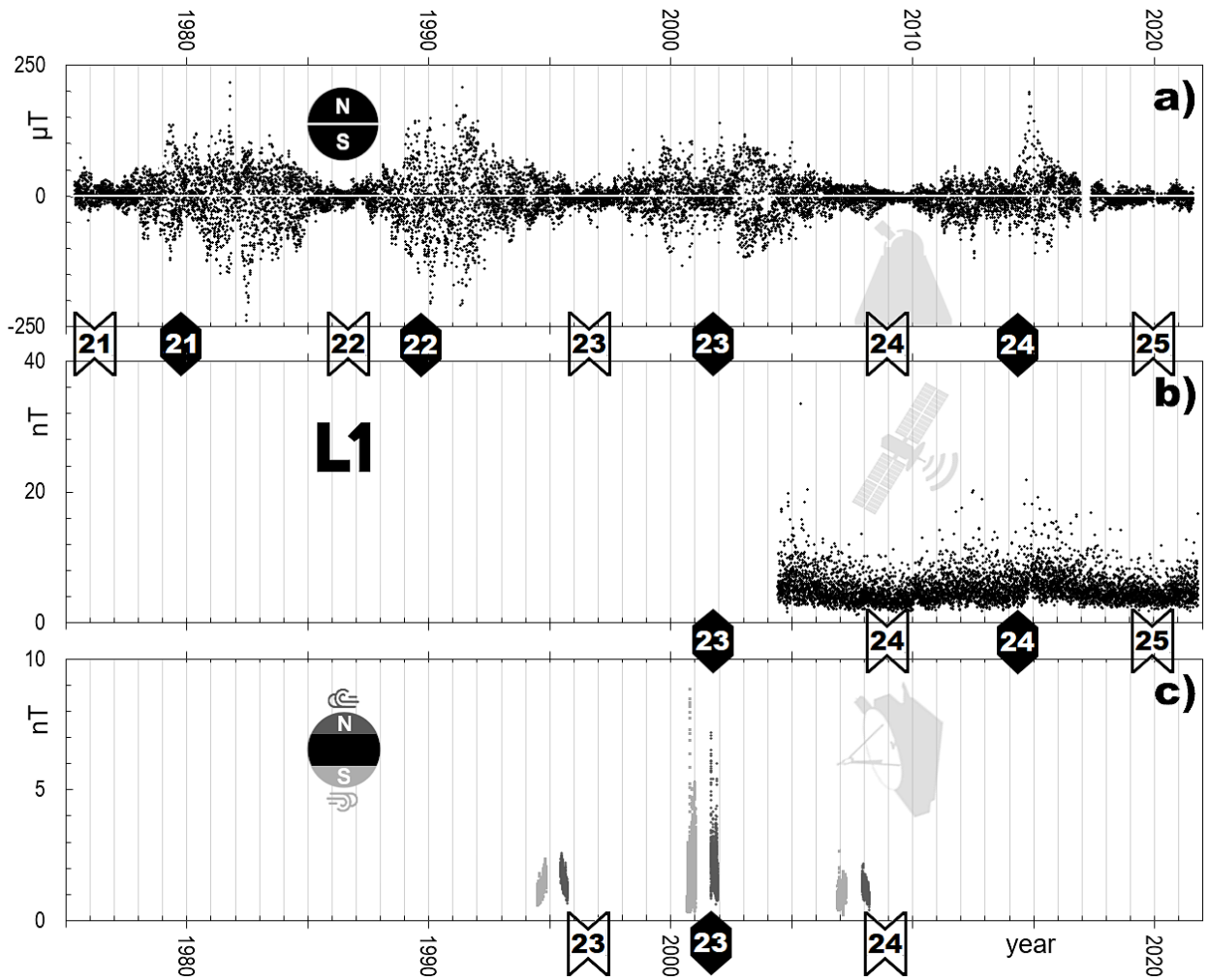


Figure 1. Plots of analyzed average strengths, B , of magnetic fields studied. Panel a: daily averages of the Sun's $B \leq 150 \mu\text{T}$ mean magnetic field (MMF) by the Wilcox Solar Observatory/ telescope (WSO) from 16 May 1975–03 August 2021. Panel b: daily averages of the $B \leq 50 \text{ nT}$, 2004–2021 interplanetary magnetic field (IMF) by WIND at the L1 Lagrangian point from 01 June 2004–04 November 2021. Panel c: hourly averages of the $B \leq 10 \text{ nT}$ IMF from Ulysses over the Sun's polar regions ($\varphi_{\text{Sun}} > |70^\circ|$) in three flybys above the southern (light gray): 26 June–05 November 1994, 6 September 2000–16 January 2001, 17 November 2006–03 April 2007, and the northern polar region (dark gray): 19 June–29 September 1995, 31 August–10 December 2001, 30 November 2007–15 March 2008. As can be seen already here in the time domain, the IMF both at L1, panel b, and over the Sun's polar regions, panel c, not only acts in unison with solar cycles of magnetic activity's maxima and minima but also closely resembles usual year-to-year activity. Thus the IMF largely preserves years-long systematic contents, thus prompting for decade-scale spectral analyses of the data down to the solar cycle's Schwabe period, $P_S \sim 11 \text{ yr}$. IMF observations by WIND in the lunar orbit, from 01 January 1995–31 May 2004, i.e., before assuming the mission target orbit at L1, were omitted from computations and the plot for clarity. Numbered arrows mark the times of respective solar cycles that by convention always start at a minimum activity (shown as white arrows) and develop into a maximum solar activity (as black arrows) around midway through the respective cycle. To compensate for a relatively lower data resolution in polar data vs. other datasets, hourly averages of the Ulysses samplings, panel a, presumably richer in systematic information than daily averages, were used. Data were plotted co-temporally amongst the panels for comparison, and are given in the Supplement.

The lead resonance period of the north wind in this condensed band was $P_S = 12.0 \text{ yr}$, panel e. Even though this northern data spectrum somewhat outperformed the southern, panel d, due to relatively higher levels of southern turbulence and the temporal proximity of solar cycles' activity extremes to the north samples, Fig.1, all periods for both polar regions are $\geq 99\%$ significant, and in terms of resonance and antiresonance (due to coupling) trains were resolved. The 9–11-yr periods difference itself, as a consequence of polar asymmetry in the solar magnetic activity, can be expected to trigger a perfect (integer-ordered) mechanical resonance in the wind's waving, here recovered in both polarities, as shown in Fig. 2

over the 1–13-yr (31.710–2.439-nHz) condensed spectral band. As opposed to turbulence that exhibits smooth spectra, such a perfect resonance can only be dictated by the Sun internally; see, e.g., Gough (1995), here especially so since characterized by sharp peaks and troughs, and very high fidelity — all indications of a deterministic driving process. This result agrees with Knaack and Stenflo (2005), who claimed that ~1-yr and longer Sun periodicities align to solar cycles and are unlikely to arise randomly. Note here that the Ulysses hourly data contained presumably more complete systematic information and have outperformed the WIND and WSO data despite the latter two records featuring relatively higher completeness rates and longer time spans. The significant variation between the spectral magnitudes of resonance peaks in panels e vs. d of Fig. 2 reflects the N–S asymmetry in solar-wind IMF, found affecting wind speeds and confirmed independently of Ulysses data, e.g., by Tokumaru et al. (2015).

For a more detailed insight into the AR and RR, and since AR is driven presumably by the Schwabe cycle (Alfvén, 1943), the spectra of data from Fig. 1 were re-computed (“zoomed out”) in the 1-month–13-yr (385.802–2.439-nHz or 1200.00–7.69-cycles per century) full band of subrotational frequencies, or in the 0.01–1.60 ZeV ($\sim 1.6 \cdot 10^7$ – $2.5 \cdot 10^9$ erg) full band of energies. This approach is further justified by Fig. 2–d & e already matching experimental results, Fig. 7–a. The results are in Tables 1–3 and Fig. 3 on five panels, again respective to the panels of Fig. 1 and the five panels of Fig. 2. As in Fig. 2, the MMF in Fig. 3, panel a, and the N–S combined data, panel c, reveal that spectra tend to flatness due to turbulence (Gough, 1995). However, despite a heavy turbulence suppression, equatorial instability never attenuates the (fast-wind) resonance entirely, as seen in the partial and 0.1-var% faint extraction of RR at 67%+ significance, panel a. (Here, well-known physical processes are regarded as significant if extracted with at least 67% significance.) Furthermore, any radical disparity amongst the P_s global resonance modes, Fig. 2, is now gone, Fig. 3, and those periods are now more congruent, as discussed later. Note an improvement in the estimates of P_s and P_{Rg} periods going from panels a–e here and from Fig. 2–e to Fig. 3–e, as well as in the spectral resolution of the Rieger resonance (extraction-wise and magnitude-wise), seen as a relative increase in the left-hand frame’s area with data separation. Also seen is a magnitude-of-order increase in spectral magnitudes on panels c–e compared to a & b, i.e., in system-energy bands occupied by AR, meaning the P_{Rg} from panel a (value grayed out), while 67%-significant, is still part of background noise and thus not emitted equatorially. Panel b of Fig. 3 has revealed from WIND spacecraft measurements of the IMF at L1 that the heliosphere maintains AR and RR at least to L1 distances, each as a whole. However, this pureness of the signal breaks down temporally beyond/above the antiresonance train’s termination point at ~annual periodicity (at which the global coupling ceases but without vibration relaxation), spatially beyond L1, thus leaving RR open to external influences ranging from planetary constellations and gravitation to increased activity of magnetic fields, all suggested in the past.

As seen from Figs. 2–e and 3–e, the couplings-free RR is a re-emitted (offshoot of) AR via the tailing antiresonance mode P_{17} , and primarily around the extremal phases, i.e., maxima and minima, when conditions least favor turbulence (depicted in frequency space as anisotropic peak-splitting), making room for a partial reorganization of the fields’ activity into resonance and antiresonance trains. Note the original, i.e., system value of P_{Rg} as released by the Sun during the solar cycle 23 maximum, Fig. 1, of 156.5 days. The fluctuation in P_{Rg} throughout the heliosphere is constrained to no more than a few % of P_{Rg} and seen formatted into the above-mentioned Rieger-type harmonics. Namely, this limited variability in RR is an additional indicator of a possible impact of interplanetary constellations, including planetary gravitation and magnetism (since those are geodynamically most significant, as experienced by the solar system bodies), on P_{Rg} and the couplings-freed RR that thus gets reformatted into Rieger-type periodicities as reported widely. Fidelity values stayed well below 12 on all peaks of RR (when RR is computed alone, i.e., in the 30–180-day band; not shown), revealing that RR as part of the Sun’s AR signal is never a solitary, i.e., uncoupled physical process. Thus as soon as it gets released from the Sun couplings, factors external to the Sun, like the above-mentioned planetary constellations including planetary gravitation and magnetism, take over in the role of additional actors in suppressing the fidelity on peaks down to ~annual termination modes.

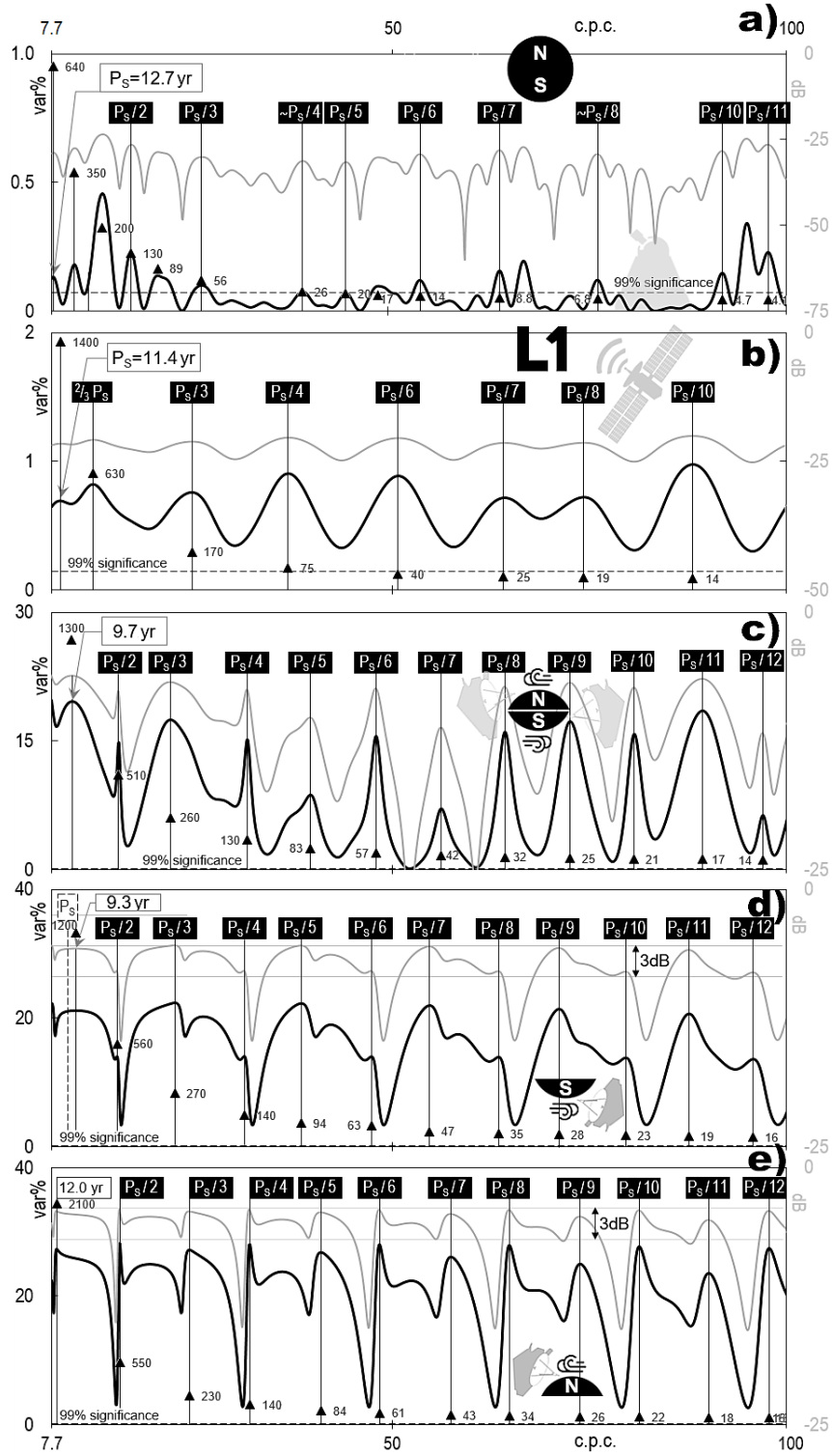


Figure 2. GV spectra of magnetic fields' strength variations from Fig. 1 reveal the $P_s \approx 11$ -yr (Schwabe) mode-driven *a-mode* (Alfvén) resonance (AR) in the 100.00–7.69 cycles per century (c.p.c.), i.e., 1–13 yr or 365–4745 days (31.710–2.439-nHz) band. Panel a — from WSO-derived daily values of the MMF; panel b — from the WIND spacecraft's quasi-stationary IMF samplings at L1; panel c — from Ulysses flybys over the Sun's polar regions; panel d — separately from Ulysses magnetometer data over the northern; and panel e — separately from Ulysses magnetometer data over the southern polar region. Numbered triangles mark the fidelity values on respective spectral peaks along a third arbitrary vertical axis (not shown). Fidelity on extracted spectral periodicities stayed well above 12, indicating a genuinely dynamical process (Omerbashich, 2006). Note the overall increase in statistical fidelity following the N–S data separation and the increase in system energy occupied by AR, from ~ 10 var%, panel c, to ~ 20 var%, panel d, and ~ 25 var%, panel e. In addition, the mutual resemblance of variance and power spectra, which virtually coincide in shape, indicate that the Fig. 2 spectra describe happens over far wider bands, which warrants re-computing spectra. Indeed, the results of spectra recomputation, now in the Sun full long-period band (of rotational-to-Schwabe frequencies), were plotted in Fig. 3. Note that the mode order in the present study is per separate extractions as shown in Tables 1 (marked as m), 2 (marked as k), and 3 (marked as n), rather than imagining the symmetrical (parity-dependent) Sun in simple modeling such as spherical decomposition.

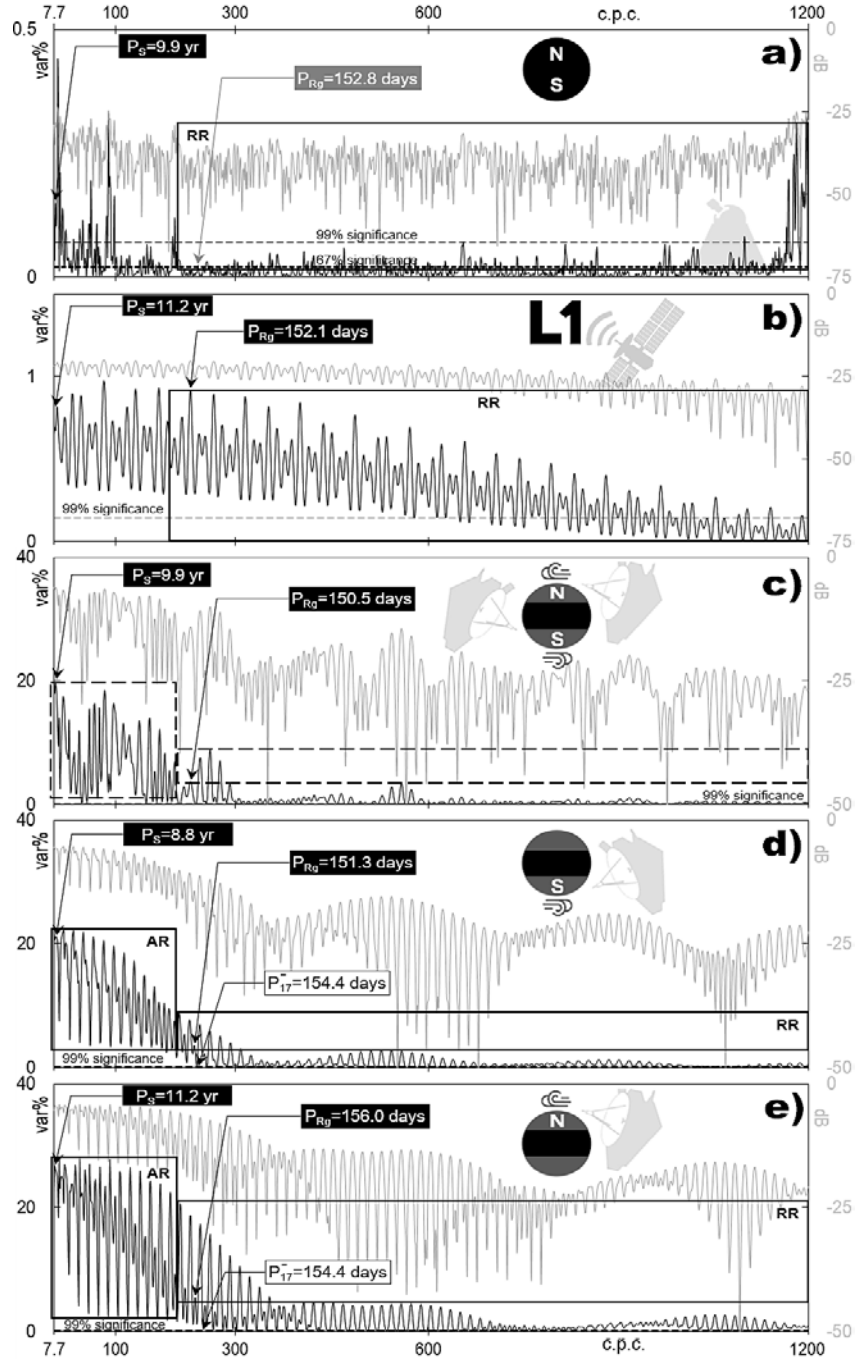


Figure 3. GV spectra of data, Fig. 1, in the 1200.00–7.69 c.p.c., i.e., 1-month–13 yr or 30–4745 days (385.802–2.439-nHz) band of Sun subrotational frequencies, revealing complete AR in some cases, i.e., a continuous spectrum of modes. Panel a — AR absence from the MMF; panel b — AR detection in the IMF at L1 from WIND; panel c — AR extraction from the northern- and southern polar wind data combined; panel d — AR extraction from the northern polar wind data; panel e — AR extraction from the southern polar wind. The left-hand frame, labeled as AR (note the AR proper includes within its 30–180-day subband the RR as well), partly seen in Fig. 2, delimits the main (0.5–13-yr) frequency subband of highest resonantly magnified energies in the Sun vibrations, as seen from intensive and systematic peak-splitting due to coupling but not turbulence anisotropy, which thus turns out to have been moderated by AR. The right-hand frame delimits the 30–180 days frequency subband of the Rieger resonance (RR) under the $P_{Rg} \sim 154$ -day Rieger mode, widely reported in solar indices and which here turns out to be a subband of AR global resonance, Fig. 2. P_{Rg} estimates recover best from the IMF at L1 (WIND), panel b, and northern-polar IMF, panel e, reflecting the known fact that primarily the northern fast solar wind reaches the IMF at L1. Thanks to GVSA spectral magnitudes in var% being directly proportionate to system energy, the resonances are extracted fully (with a continuous spectrum of modes and complete with antiresonances and patterns in both parities) so that frames scale also magnitude-wise, i.e., as energy bands. Fidelity (not shown) satisfied the $\Phi > 12$ threshold for periods of up to ~ 1 -yr, indicating that the AR spectrum represents a genuine process, here up to the \sim annual cycle(s), exposing RR as not a self-sustained physical process but a carrier of the Sun’s resonance frequency (P_s global resonance mode) and its (by couplings superimposed) antiresonance harmonics. Thus the real (gravitationally unperturbed) P_{Rg} is extracted as $P_{17} = 154.4$ -day from both polar regions, panels d & e and Table 2. Note AR as always preceded by an antiresonance mode P^* , which also holds for P_0 when the band’s lower limit gets lowered even further, say to 5 c.p.y. (not shown). The period labels highlighted in gray mark a (67–99%)-confidence. Frame labels omitted for clarity where necessary, and frames dashed where resonance driver is absent. Numerical values of the plotted AR modes are listed in Table 1 and of antiresonance modes in Table 2. Notably, the Sun vibrates at all times with three global modes: the original P_s northwards plus two variations, a ~ 9 -yr southwards and a ~ 10 -yr equatorially, panels e/b, d, c/a, respectively.

The complete extraction of AR and RR explains why the Rieger period P_{Rg} is so profoundly present throughout our solar system. Namely, P_{Rg} is the last $\geq 99\%$ -significant antiresonance mode, of order $k=17$, at whose frequency the internal global couplings cease, and this P_{17} mode remains the shortest a-mode produced by the Sun alone, allowing this mode, as the real, i.e., externally-gravitationally still unperturbed P_{Rg} , to effectively escape the Sun's inherent anisotropy and turbulence. Once set free (becoming exposed to planetary fields, mainly gravitational but in case of gaseous giants magnetic, perturbations), dynamical waves in the solar ejecta that propagate under the P_{17} mode create at least two reflection trains complete with resonances but without antiresonances (the Sun internal couplings) anymore and up to the rotational frequencies, Figs. 2–4. This composition reveals RR as an actor in the solar-system dynamics, in unison with planetary gravitational and magnetic fields. The $P_{17} = 154.4$ days, as one of only two a-modes obtained from both the southern- and northern polar fast wind Ulysses data separately, Table 3, thus appears in various types of heliophysical data as a prevailing driver that guides the from-that-point-on released wind's principal mechanism of propagation — the quasiperiodic flapping about the ecliptic. At the same time, P_{Rg} becomes the carrier wave of the power from all the preceding (lower) frequencies below P_s , namely the AR train. Thus P_{Rg} is locked firmly in-between the two dominant global dynamical regimes (internally: that of AR; externally: that of planetary constellations and fields), making it overall the most present resonance mode in the heliosphere, which is already well known to be the case, see Introduction. As seen from Figs. 4 & 5, fidelity drops to $\Phi < 12$ beyond the antiresonances termination, i.e., in sup-annual frequency bands, allowing further for the possibility that RR becomes modulated by planetary constellations and fields; e.g., the Hale cycle too could be modulated by heliosphere's magnetism (Thomas et al., 2014). This flexibility means that from P_{Rg} on, fields couple freely with P_{Rg} waves as the otherwise final (antiresonances-termination-) offshoot of AR. Here the AR's power gets channeled in the heliosphere by a gravitomagnetically modified RR (physical waves of solar ejecta) pushed outwards resonantly and thereby sped up, which is known to occur at least until the wind reaches $\sim 10R_\odot$ but lacked explanation until now (Grail et al., 1996). Thus the Rieger period is simply a triple (tri-band) resonance response of the Sun to its three significantly contrarian global vibrations (~ 11 , ~ 10 , ~ 9 -yr) around the global mode: $P_{Rg} = P_s/3/3/3$.

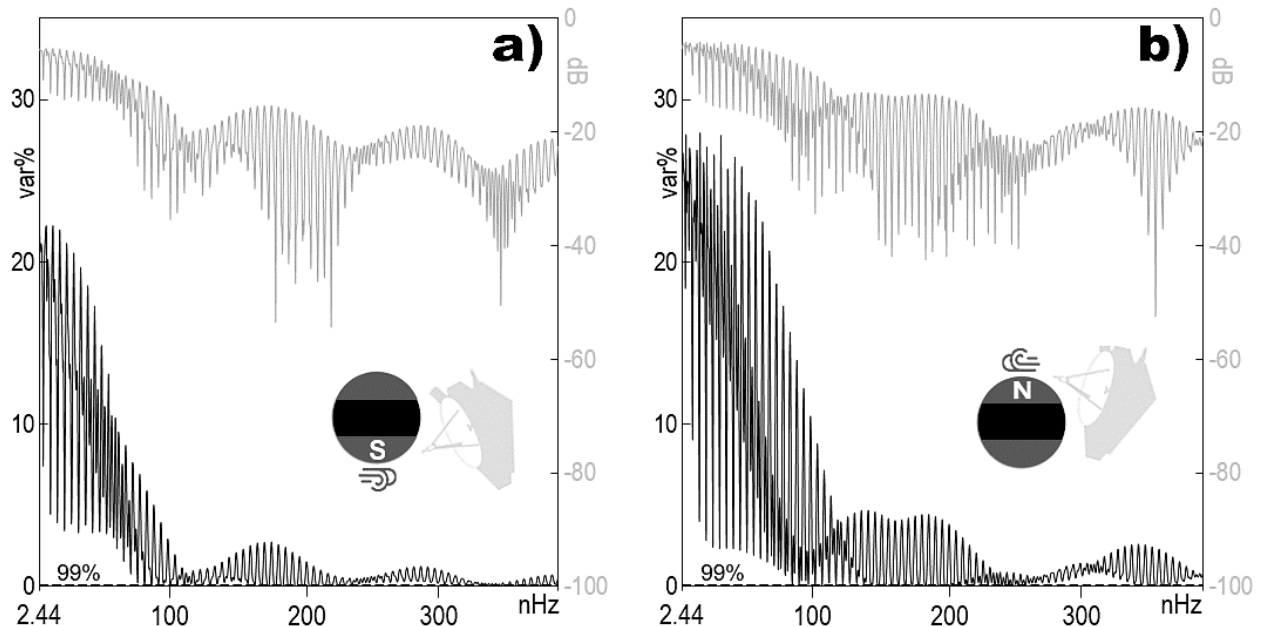


Figure 4. A compressed view of AR, highlighting waveform envelopes: in the southern polar fast wind from Fig. 3–d, panel a, and in the northern polar fast wind from Fig. 3–e, panel b. Fig. 3–e.

m	WSO MMF		WIND IMF/L1		Ulysses NS		Ulysses S		Ulysses N		m	WSO MMF		WIND IMF/L1		Ulysses NS		Ulysses S		Ulysses N		
	P _m	Φ _m		P _m	Φ _m																	
0	3609.3	390	4100.0	1300	3609.3	1300	3223.6	1100	4100.0	1800	66			44.1	0.2	55.2	0.3	59.4	0.4	64.7	0.5	
1	2655.9	210	2912.3	670	2258.2	510	1558.2	260	2258.2	550	67			43.4	0.2	53.9	0.3	57.9	0.4	62.9	0.4	
2	2100.9	130	1481.6	170	1643.1	270	1349.1	200	1844.0	370	68			42.7	0.1	53.0	0.3	56.4	0.3	61.3	0.4	
3	1737.7	89	993.6	78	1144.3	130	932.1	93	1481.6	240	69			42.1	0.1	52.4	0.3	55.0	0.3	59.7	0.4	
4	1349.1	54	712.1	40	904.2	82	853.0	78	1102.5	130	70			41.5	0.1	51.7	0.3	53.6	0.3	58.2	0.4	
5	932.1	26	565.3	25	766.3	59	766.3	63	993.6	110	71			40.9	0.1	51.1	0.3	52.3	0.3	57.5	0.4	
6	747.4	17	491.6	19	650.6	42	665.0	47	877.9	83	72			40.3	0.1	50.5	0.3	51.1	0.3	56.8	0.4	
7	680.0	14	416.8	14	565.3	32	623.7	42	747.4	60	73			39.8	0.1	50.0	0.3	50.3	0.3	56.1	0.3	
8	565.3	10	357.5	10	499.7	25	576.1	36	695.6	52	74			39.3	0.1	49.4	0.2	49.9	0.3	55.4	0.3	
9	544.8	9	323.1	8	454.5	21	516.8	29	636.9	44	75			38.7	0.1	48.8	0.2	49.3	0.3	54.8	0.3	
10	476.0	7	291.8	7	411.2	17	461.5	23	565.3	34	76			38.2	0.1	48.3	0.2	48.8	0.3	54.1	0.3	
11	395.0	5	263.7	6	380.1	14	416.8	19	491.6	26	77			37.8	0.1	47.5	0.2	48.2	0.3	53.5	0.3	
12	384.9	4	240.6	5	353.4	12	384.9	16	447.8	22	78			37.3	0.1	47.1	0.2	47.8	0.2	52.9	0.3	
13	375.3	4	226.2	4	306.6	9	353.4	13	405.6	18	79			36.7	0.1	46.7	0.2	47.2	0.2	52.2	0.3	
14	349.3	4	207.5	3	283.6	8	326.6	11	375.3	15	80			35.9	0.1	46.2	0.2	46.7	0.2	51.7	0.3	
15	184.6	1	192.9	3	252.7	6	303.6	10	345.3	13	81			35.4	0.1	45.3	0.2	46.2	0.2	51.1	0.3	
16	181.3	1	182.4	3	238.7	6	286.3	9	323.1	11	82			34.2	0.1	44.6	0.2	45.7	0.2	50.6	0.3	
17	55.0	0	171.0	2	226.2	5	268.4	8	300.5	10	83			33.0	0.1	43.9	0.2	45.3	0.2	50.0	0.3	
18	32.8	0	161.0	2	216.4	5	254.8	7	280.9	9	84			32.6	0.1	43.1	0.2	44.8	0.2	49.5	0.3	
19	30.9	0	152.1	2	206.1	4	238.7	6	266.1	8	85			31.6	0.1	42.3	0.2	44.5	0.2	48.9	0.3	
20	30.8	0	146.2	2	196.7	4	229.6	6	250.6	7	86			30.3	0.1	41.9	0.2	43.9	0.2	48.5	0.3	
21	30.6	0	138.1	2	189.3	4	216.4	5	236.8	6	87					41.5	0.2	43.1	0.2	47.9	0.3	
22	30.5	0	131.5	1	181.3	3	207.5	5	224.5	5	88					41.1	0.2	42.2	0.2	47.5	0.2	
23	30.3	0	126.0	1	169.1	3	198.0	4	214.9	5	89						40.5	0.2	41.5	0.2	47.0	0.2
24	30.2	0	121.4	1	161.0	3	190.5	4	204.7	5	90						39.9	0.2	40.7	0.2	46.5	0.2
25	30.1	0	116.3	1	150.5	2	182.4	4	196.7	4	91						39.3	0.2	40.0	0.2	46.0	0.2
26			111.1	1	146.2	2	175.0	3	188.1	4	92						38.7	0.2	39.3	0.2	45.6	0.2
27			108.0	1	141.4	2	168.2	3	181.3	4	93						38.1	0.1	38.6	0.2	45.1	0.2
28			103.9	1	137.5	2	162.7	3	174.0	3	94						37.5	0.1	38.0	0.2	44.7	0.2
29			100.1	1	133.2	2	156.8	3	168.2	3	95						37.0	0.1	37.4	0.2	44.3	0.2
30			96.6	1	129.8	2	151.3	3	161.0	3	96						36.7	0.1	36.8	0.1	43.9	0.2
31			93.9	1	126.0	2	146.9	2	156.0	3	97						36.4	0.1	36.2	0.1	43.5	0.2
32			90.7	1	120.0	1	141.4	2	150.5	2	98						36.1	0.1	36.1	0.1	43.0	0.2
33			87.8	1	117.2	1	137.5	2	146.2	2	99						35.8	0.1	35.7	0.1	42.8	0.2
34			85.6	1	114.1	1	133.2	2	141.4	2	100						35.6	0.1	35.4	0.1	42.2	0.2
35			83.0	1	110.7	1	129.8	2	137.5	2	101						35.2	0.1	35.1	0.1	42.0	0.2
36			80.6	1	108.0	1	125.5	2	133.2	2	102						34.7	0.1	34.9	0.1	41.3	0.2
37			78.5	0.5	105.3	1	121.9	2	129.8	2	103						34.3	0.1	34.6	0.1	40.6	0.2
38			76.7	0.5	102.8	1	119.0	2	126.0	2	104						33.8	0.1	34.3	0.1	39.9	0.2
39			74.4	0.4	100.8	1	115.4	1	122.9	2	105						33.5	0.1	34.1	0.1	39.4	0.2
40			72.4	0.4	98.1	1	112.8	1	119.5	2	106						33.2	0.1	33.8	0.1	39.2	0.2
41			70.9	0.4	95.3	1	109.5	1	116.7	2	107						32.7	0.1	33.5	0.1	38.8	0.2
42			69.3	0.4	93.3	1	107.2	1	113.7	1	108						32.2	0.1	33.3	0.1	38.5	0.2
43			67.6	0.4	91.3	1	104.6	1	111.1	1	109						31.7	0.1	33.1	0.1	38.2	0.2
44			65.9	0.3	89.4	1	102.1	1	108.4	1	110						31.4	1.0	32.8	0.1	37.9	0.2
45			64.7	0.3	87.6	1	99.8	1	106.1	1	111						31.2	1.0	32.6	0.1	37.5	0.2
46			63.2	0.3	85.8	1	97.5	1	103.5	1	112						31.0	1.0	32.3	0.1	37.3	0.2
47			61.8	0.3	84.2	1	95.6	1	101.4	1	113						30.8	0.9	32.1	0.1	36.9	0.2
48			60.6	0.3	83.0	1	91.6	1	99.1	1	114						30.5	0.9	31.9	0.1	36.6	0.1
49			59.3	0.3	80.8	1	87.6	1	97.2	1	115						30.1	0.9	31.6	0.1	36.4	0.1
50			58.1	0.3	78.1	1	85.6	1	95.0	1	116								31.2	0.1	36.1	0.1
51			56.9	0.3	75.5	1	84.2	1	93.3	1	117								30.8	0.1	35.8	0.1
52			56.0	0.3	74.2	1	82.6	1	91.3	1	118								30.3	0.1	35.3	0.1
53			54.8	0.2	73.1	1	81.2	1	89.4	1	119										34.7	0.1
54			53.7	0.2	72.1	1	79.7	1	87.8	1	120										34.2	0.1
55			52.9	0.2	70.1	0.5	78.3	1	86.1	1	121										33.7	0.1
56			52.0	0.2	68.3	0.5	76.9	1	84.6	1	122										33.2	0.1
57			50.9	0.2	66.5	0.4	75.5	1	83.0	1	123										32.7	0.1
58			50.0	0.2	64.7	0.4	74.4	1	81.7	1	124										32.3	0.1
59			49.3	0.2	62.9	0.4	73.1	1	80.1	1	125										31.8	0.1
60			48.5	0.2	61.3	0.4	70.7	1	77.5	1	126										31.4	0.1
61			47.5	0.2	59.9	0.4	68.6	1	75.0	1	127										31.0	0.1
62			46.9	0.2	59.2	0.4	66.5	0.5	72.8	1	128										30.8	0.1
63			46.2	0.2	58.2	0.3	64.7	0.5	70.6	1	129										30.6	0.1
64			45.4	0.2	57.9	0.3	62.8	0.4	68.5	1	130										30.4	0.1
65			44.6	0.2	56.7	0.3	61.1	0.4	66.5	0.5	131										30.2	0.1

Table 1 The Sun's global-vibrational a-modes including Alfvén resonance (AR) in the raw form (anisotropic peak splitting inclusive), and the original Rieger resonance (RR) (as just freed from Sun-internal couplings) of order m, as periods P_m of ≥99%-significant peaks in G-V spectra of (columns from left to right): the Sun's MMF (WSO), the IMF at L1 (WIND), the IMF above the Sun's polar (φ_{sun}>|70°|) regions combined (Ulysses NS), and separately the IMF above the Sun's southern (Ulysses S) and northern polar region (Ulysses N). The spectral peaks with values listed compose complete AR trains in some cases, i.e., a continuous spectrum of modes, Fig. 3. Values of order m, corresponding to fidelities Φ_m≥12 indicative of a genuine systematic process (Omerbashich, 2006), are highlighted gray. RR a-modes highlighted black. Note that the present study succeeded in extracting AR to at least order m=131 from Ulysses samplings of the IMF in both-polar fast winds, Table 1, but even a resolution this high might be improved on in the future as new data become available.

The verification has thus turned out positive since both the lead period estimates and the relative change in energy bands when going from southern to northern data were reproduced successfully. This confirmation of the same result from two independent datasets of different origins and of significantly varying resolution and time-span corroborates Gough (1995) on spectra/processes under turbulence tending to flatness, so that the global, decade-scale AR is not a feature exclusive to the fast solar wind, but one that originates in the Sun instead.

P_k	Ulysses IMF-S			Ulysses IMF-N		
	[days]	[yr]	[var%]	[days]	[yr]	[var%]
2	2258.2	6.19	7.44	2440.9	6.69	18.39
3	1102.5	3.02	4.47	1144.3	3.14	9.37
4	747.4	2.05	4.19	766.3	2.10	4.62
5	554.9	1.52	3.45	576.1	1.58	3.37
6	447.8	1.23	3.94	461.5	1.26	2.91
7	370.7	1.02	3.33	384.9	1.05	2.68
8	316.3	0.87	3.81	330.1	0.90	2.53
9	278.3	0.76	3.34	289.0	0.79	2.40
10	246.5	0.68	3.43	257.0	0.70	2.26
11	222.8	0.61	3.28	231.4	0.63	2.10
12	201.9	0.55	3.04	210.4	0.58	1.92
13	194.1	0.53	2.35	192.9	0.53	1.71
14	179.1	0.49	1.61	178.1	0.49	1.50
15	171.0	0.47	2.47	165.4	0.45	1.29
16	165.4	0.45	0.82	158.4	0.43	1.12
17	154.4	0.42	0.24	154.4	0.42	1.11
18	144.8	0.40	0.09	138.8	0.38	0.14
	99%@: 0.10			99%@: 0.13		

Table 2. GVSA extraction of Sun global Alfvén antiresonance, Figs. 3 & 4, from Ulysses measurements of IMF over the southern polar (left-hand side; Ulysses IMF-S) vs. northern polar (right-hand side; Ulysses IMF-N) regions of the Sun. All extracted periods are $\geq 99\%$ -significant, with antiresonance P_k modes accompanying (always preceding) P_m (i.e., AR), Table 1, up to the order $k=18$, at which point the significance drops below 99% (gray values in the last row). Note the original (as generated under the Sun couplings) Rieger period (highlighted black), $P_{17}=154.4$ days was one of only two modes extracted with the same value from both polar data sets, i.e., the Ulysses samplings of polar regions separated into the southern- and northern-polar time series. The Sun couplings give rise to the antiresonance, while such a strong signal at this mode is the reason behind this antiresonance mode's vast presence in solar indices and its confusion for a Sun's resonance period.

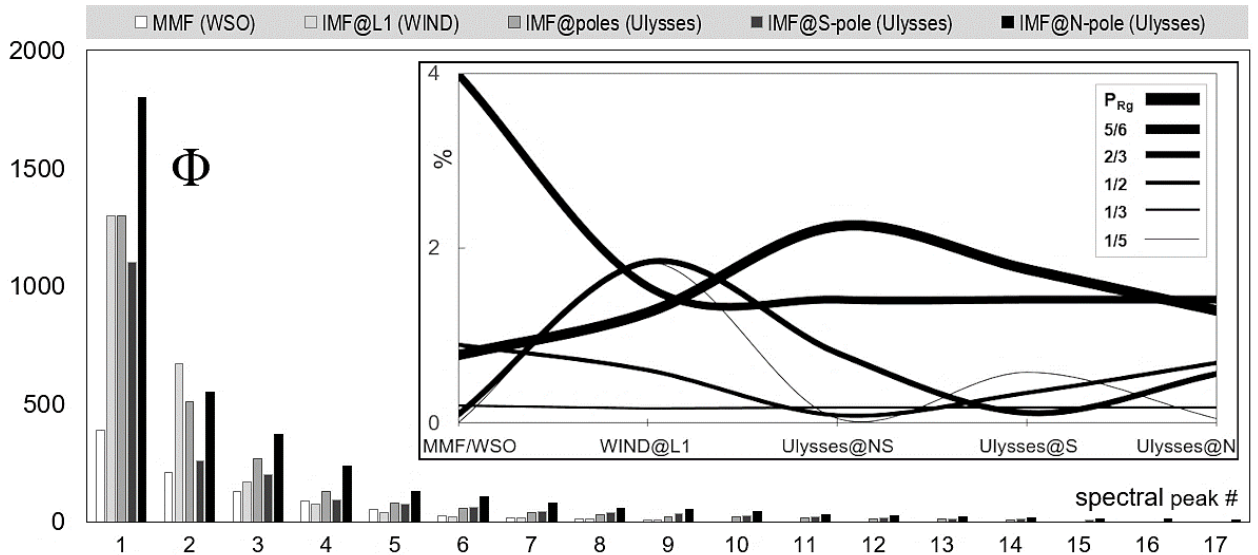


Figure 5. Change in significant fidelity, $\Phi \geq 12$, with a computed spectral peak, up to the first 16 harmonics (highlighted gray in Table 1) plus an additional value, going from the MMF (white bars), IMF at L1 (light gray bars), IMF at polar regions combined (gray bars), IMF at the southern polar region (dark gray bars), to IMF above the Sun's northern polar region (black bars). The last shown value #17 corresponds to \sim annual harmonic(s) in the analyzed data sets and marks the antiresonances' (global-couplings) termination point in the frequency space. The plot reveals that the northern fast wind preserved the resonance signature the best, i.e., 15 out of 16 first (lowest-frequency) a-modes. Note that the periods shown ordered were grouped for convenience only, so the clusters as depicted neither have physical meaning nor do they necessarily refer to the same harmonics. *Callout:* consistency plot, in the matchings of the GVSA-extracted train of RR a-modes (P_{Rg} and Rieger-type periodicities), Table 1, revealing $\frac{1}{2}P_{Rg} = \sim 51$ -day as the most consistently recovered (most stable) a-mode of RR, as 51.1-day, at 0.2% across all data sets (at $\geq 99\%$ -significance from the four polar-wind data sets). Most of the extracted RR a-modes were well within $\sim 2\%$ of respective Rieger modes; see Introduction for the most commonly reported values of the Rieger train modes, here taken as reference values for computing the matchings (in %). All matchings were for $\geq 99\%$ -significant periods, except for the MMS WSO data, for which the RR train was extracted with [67%, 89%), [89%, 95%), [89%, 95%), [95%, 99%), [95%, 99%), [89%, 95%), and [95%, 99%) significance going from P_{Rg} to its highest harmonic, respectively. The matchings reflect the known fact that the equatorially mixed wind is overall slower than the polar (mostly fast) wind, and therefore unable to maintain the ever-dissipating signature of the Sun resonance (as the manner of wind ejection) as the considerably faster polar wind can, Figs. 2–e and 3–e.

n	$^S P_{\text{meas}}$	$^S P_{\text{theor}}$	$^S \Delta$	n	$^S P_{\text{meas}}$	$^S P_{\text{theor}}$	$^S \Delta$	n	$^N P_{\text{meas}}$	$^N P_{\text{theor}}$	$^N \Delta$	n	$^N P_{\text{meas}}$	$^N P_{\text{theor}}$	$^N \Delta$
1	3223.6			51	62.8	63.2	0.7%	1	4100.0			51	80.1	80.4	0.3%
2	1558.2	1611.8	3.3%	53	61.1	60.8	-0.5%	2	2258.2	2050.0	-10.2%	53	77.5	77.4	-0.1%
3	932.1	1074.5	13.3%	54	59.4	59.7	0.4%	3	1481.6	1366.7	-8.4%	55	75.0	74.5	-0.6%
4	766.3	805.9	-5.9%	56	57.9	57.6	-0.5%	4	993.6	1025.0	3.1%	56	72.8	73.2	0.6%
5	665.0	644.7	-3.1%	57	56.4	56.6	0.2%	5	877.9	820.0	-7.1%	58	70.6	70.7	0.2%
6	516.8	537.3	3.8%	59	55.0	54.6	-0.7%	6	695.6	683.3	-1.8%	60	68.5	68.3	-0.2%
7	461.5	460.5	-0.2%	60	53.6	53.7	0.2%	7	565.3	585.7	3.5%	62	66.5	66.1	-0.6%
8	416.8	402.9	-3.4%	62	52.3	52.0	-0.6%	8	491.6	512.5	4.1%	64	64.7	64.1	-1.0%
9	353.4	358.2	1.3%	63	51.1	51.2	0.2%	9	447.8	455.6	1.7%	65	62.9	63.1	0.2%
10	326.6	322.4	-1.3%	64	50.3	50.4	0.1%	10	405.6	410.0	1.1%	67	61.3	61.2	-0.1%
11	303.6	293.1	-3.6%	65	49.9	49.6	-0.6%	11	375.3	372.7	-0.7%	69	59.7	59.4	-0.4%
12	268.4	268.6	0.1%	66	49.3	48.8	-0.8%	12	345.3	341.7	-1.1%	70	58.2	58.6	0.7%
13	254.8	248.0	-2.8%	67	48.2	48.1	-0.2%	13	323.1	315.4	-2.4%	71	57.5	57.7	0.4%
14	229.6	230.3	0.3%	68	47.8	47.4	-0.8%	14	300.5	292.9	-2.6%	72	56.8	56.9	0.3%
15	216.4	214.9	-0.7%	69	46.7	46.7	0.0%	15	266.1	273.3	2.7%	73	56.1	56.2	0.1%
16	198.0	201.5	1.7%	70	46.2	46.1	-0.4%	16	250.6	256.2	2.2%	74	55.4	55.4	0.0%
17	190.5	189.6	-0.4%	71	45.3	45.4	0.2%	17	236.8	241.2	1.8%	75	54.8	54.7	-0.2%
18	182.4	179.1	-1.8%	72	44.8	44.8	0.0%	18	224.5	227.8	1.4%	76	54.1	53.9	-0.3%
19	168.2	169.7	0.9%	73	44.5	44.2	-0.7%	19	214.9	215.8	0.4%	77	53.5	53.2	-0.5%
20	162.7	161.2	-1.0%	74	43.9	43.6	-0.7%	20	204.7	205.0	0.2%	78	52.2	52.6	0.6%
21	151.3	153.5	1.4%	75	43.1	43.0	-0.2%	21	196.7	195.2	-0.7%	79	51.7	51.9	0.4%
22	146.9	146.5	-0.2%	76	42.2	42.4	0.5%	22	188.1	186.4	-0.9%	80	51.1	51.2	0.3%
23	141.4	140.2	-0.9%	78	41.5	41.3	-0.3%	23	181.3	178.3	-1.7%	81	50.6	50.6	0.1%
24	133.2	134.3	0.8%	79	40.7	40.8	0.3%	24	168.2	170.8	1.6%	82	50.0	50.0	0.0%
25	129.8	128.9	-0.7%	81	40.0	39.8	-0.5%	25	161.0	164.0	1.8%	83	49.5	49.4	-0.2%
26	125.5	124.0	-1.2%	82	39.3	39.3	0.0%	26	156.0	157.7	1.1%	84	48.9	48.8	-0.3%
27	119.0	119.4	0.3%	83	38.6	38.8	0.6%	27	150.5	151.9	0.9%	85	48.5	48.2	-0.5%
28	115.4	115.1	-0.2%	85	38.0	37.9	-0.1%	28	146.2	146.4	0.2%	86	47.5	47.7	0.4%
29	112.8	111.2	-1.5%	86	37.4	37.5	0.3%	29	141.4	141.4	0.0%	87	47.0	47.1	0.4%
30	107.2	107.5	0.2%	88	36.8	36.6	-0.4%	30	137.5	136.7	-0.6%	88	46.5	46.6	0.2%
31	104.6	104.0	-0.6%	89	36.2	36.2	0.0%	31	133.2	132.3	-0.7%	89	46.0	46.1	0.1%
32	99.8	100.7	1.0%	90	36.1	35.8	-0.7%	32	129.8	128.1	-1.3%	90	45.6	45.6	-0.1%
33	97.5	97.7	0.2%	91	35.7	35.4	-0.7%	33	122.9	124.2	1.1%	91	45.1	45.1	-0.2%
34	95.6	94.8	-0.9%	92	35.1	35.0	-0.3%	34	119.5	120.6	0.9%	92	44.7	44.6	-0.4%
35	91.6	92.1	0.6%	93	34.6	34.7	0.3%	35	116.7	117.1	0.3%	93	44.3	44.1	-0.4%
37	87.6	87.1	-0.5%	94	34.3	34.3	-0.1%	36	113.7	113.9	0.2%	94	43.5	43.6	0.3%
38	85.6	84.8	-0.9%	95	34.1	33.9	-0.4%	37	111.1	110.8	-0.3%	95	43.0	43.2	0.4%
39	82.6	82.7	0.1%	96	33.5	33.6	0.1%	38	108.4	107.9	-0.4%	96	42.8	42.7	-0.1%
40	81.2	80.6	-0.8%	97	33.3	33.2	-0.2%	39	106.1	105.1	-0.9%	97	42.0	42.3	0.1%
41	78.3	78.6	0.5%	98	32.8	32.9	0.3%	40	101.4	102.5	1.0%	98	42.0	41.8	-0.5%
42	76.9	76.8	-0.2%	99	32.6	32.6	0.0%	41	99.1	100.0	0.9%	99	41.3	41.4	0.3%
43	74.4	75.0	0.7%	100	32.3	32.2	-0.4%	42	97.2	97.6	0.4%	100	40.6	41.0	1.0%
44	73.1	73.3	0.2%					43	95.0	95.3	0.3%				
46	70.7	70.1	-0.9%					44	93.3	93.2	-0.1%				
47	68.6	68.6	-0.1%					45	91.3	91.1	-0.2%				
48	66.5	67.2	0.9%					46	89.4	89.1	-0.3%				
50	64.7	64.5	-0.3%					47	87.8	87.2	-0.7%				
								48	86.1	85.4	-0.8%				
								49	83.0	83.7	0.8%				
								50	81.7	82.0	0.4%				

Table 3. Matchings of the measured $\geq 99\%$ -significant Sun AR from the Ulysses southern-polar, $^S P_{\text{meas}}$, and northern-polar, $^N P_{\text{meas}}$, data, Table 1 and Figs. 3 & 4, against theoretical-resonance periods $P_{\text{theor}}=P_1/i$, $i=2, \dots, n$; $n \in \mathbb{N}$, per the P_1 estimate of P_S from each data set, up to the order $n=100$. Matchings within $\leq 1\%$ to respective theoretical resonance periods highlighted light gray, within $\leq 1\%$ dark gray. From southern polar data, 11 theoretical-resonance periods did not have a measured match in the $\geq 99\%$ -significant spectra, and 24 of all $\geq 99\%$ -significant spectral peaks were not matched by theoretical-resonance periods, as due primarily to large-scale turbulence effects seen in spectra primarily as anisotropic peak splitting. From northern-polar data, 8 and 12, respectively. For both cases (data sets), $\sigma=0.019$. All periods in Earth days.

As seen from Table 3, while both the northern and the southern polar data performed the same in terms of perceived statistics and precision, the northern-polar data performed significantly better from the physics point of view and in terms of accuracy, recovering the theoretical resonance in more detail, seen as more successful matches by order n . Then the AR spectral signature in the northern-polar IMF appears to resemble the Sun inner workings more faithfully than the same in the southern-polar IMF. That northern

data preserved the signature of the Sun global resonance better is also seen from the symmetrical parity of theoretical a-modes that were without respective matches in the spectra. Thus the only periods missing from the northern theoretical resonance were of orders: 52, 54, then 57, 59, 61, 63, and then 66, 68 (i.e., even, even – odd, odd, odd, odd – even, even). In the spectra of the southern polar data, 36, 45, 49, 52, 55, 58, 61, 77, 80, 84, 87, indicating that some large-scale stochastic effect was overwhelmingly destroying parity in this region, most likely explained by the well-known relative instability and more extreme turbulence in the south. Thus the continuous spectrum of modes, Figs. 3 & 4, is with patterns virtually complete in both parities, to the resolution higher than 81.3 nHz (south) and 55.6 nHz (north) in the lowest frequencies and $\sim 2\mu\text{Hz}$ in most modes.

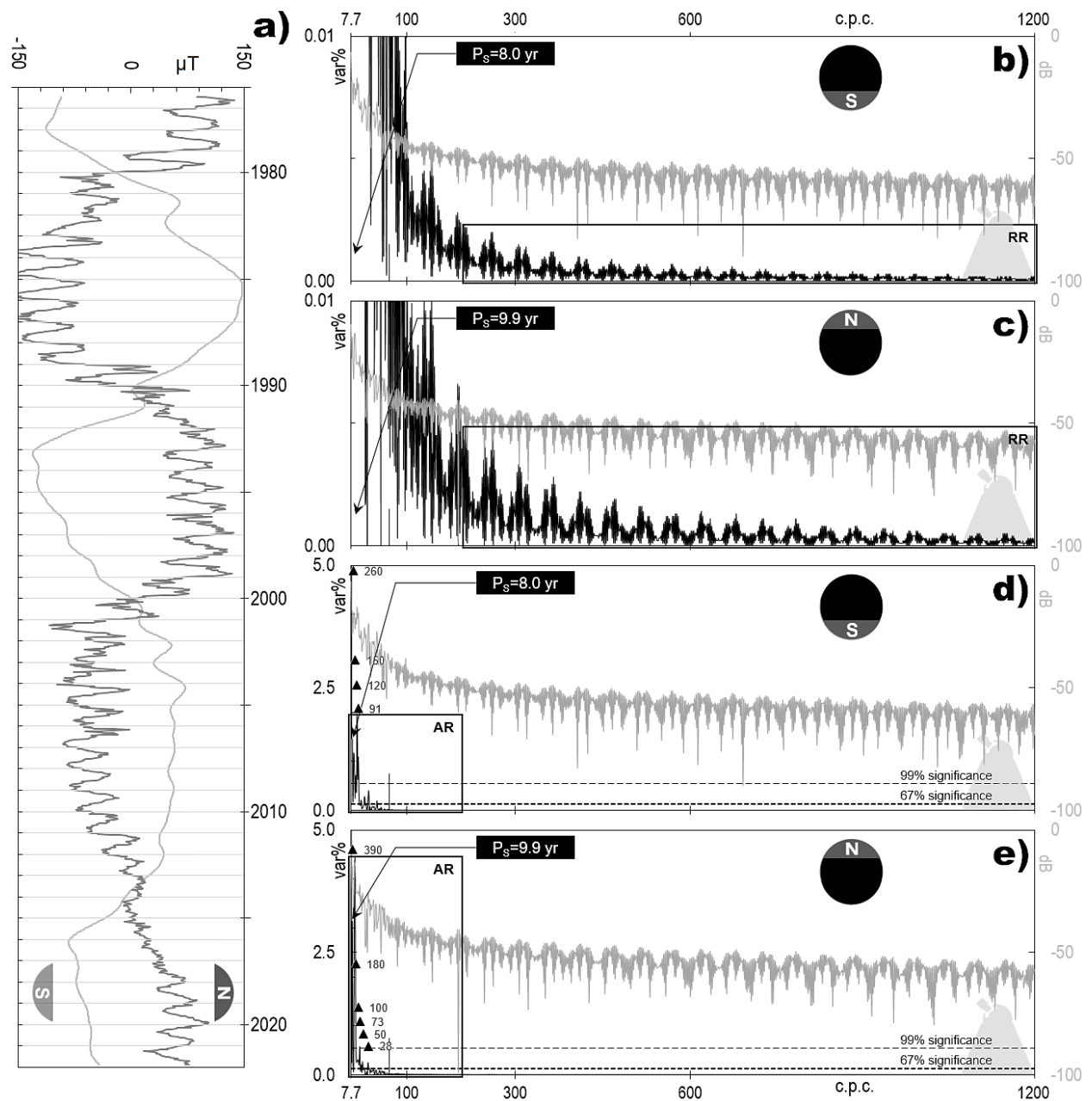


Figure 6. Verification of the main result (as obtained from Ulysses hourly averages, Fig. 3) from ten-day means of the WSO telescope's 31 May 1976–21 November 2021 polar field (PF) observations, panel a, in the same band of interest. Note that panel b depicts the same data as panel d and panel c as panel e, where panels b and d are zoomed-in along the left vertical axis to make RR visible.

As the main result of the present study, the discovery of AR and its RR offshoot from Ulysses data, Fig. 3, was verified against 1976–2021, $|B| < 150 \mu\text{T}$ WSO polar magnetic fields (PF) data, Fig. 6, to discern if perhaps the find was overstated or/and an artifact of data resolution or span, Fig.1. However, despite orders-of-magnitude differences amongst data resolution and coverage, power ratios are maintained well when going from southern to northern polar region, panels b & d vs. c & e, respectively. Then this verification is remarkable for improvement in both the detected resonances' background levels and relative energy estimates (as the area of AR and RR frames). In addition to the precision of estimates, their accuracy maintained as well: the P_s lead (mode) period, seen as degenerated likely due to fields instability, is also in remarkable agreement with (phase-shifted by -1-yr from) the same obtained for the polar regions from the Ulysses data, Fig. 3–d & e. Note that RR dropped below the 67% significance level, thus emphasizing the outcome from the Ulysses data on planetary constellations and fields as a possible cause of RR reformatting to again non-formatted trains, Fig.4, and on to modified harmonics as widely observed. Note also that the fidelity on AR is again very high ($\Phi \gg 12$), which indicates a systematic physical process discernable (although not in such high detail anymore) from the WSO telescope's polar data as from the Ulysses IMF *in situ* mission.

4. Experimental agreement

Commonly in structural and mechanical engineering, a structure's response to excitation is analyzed by studying a response model which consists of a set of frequency response functions defined over the applicable range of frequencies. Functions typically employed are the three pairs of mutual inverses: *accelerance* as the ratio of acceleration and force, *apparent mass* as the ratio of force and acceleration, *mobility* as the ratio of velocity and force, *impedance* as the ratio of force and velocity, *dynamic stiffness* as the ratio of force and displacement, and *receptance* as the ratio of displacement and force; see, e.g., Robson et al. (1971). In physical sciences, the most common way of study is the exact opposite to the engineering way above: from a description of the response properties, most commonly in the form of measured frequency response functions, deduce modal and spatial properties of a physical system. Thus, since the total response of a set of coupled components is expressible in terms of the mobility of individual components, inverse comparisons apply as well (Ewins, 1995). As we saw from the present study, the Sun is a physical system that vibrates additionally (resonates) under couplings among its latitudinally and depth-wise stratified sectors of varying physical properties. Those sectors are geographically distinct regions that exhibit significantly differential rotation rates, contrarian (out-of-phase) vibration modes and related resonances, and different mass and point velocities. The resonant response of a physical system most complete to such couplings is constructive–destructive, i.e., the one exhibiting both global resonances (characterized by sharp peaks in the system spectra) and global antiresonances (sharp troughs), Figs. 2 & 3 vs. Fig. 7. Depending on the fundamental properties of the system of interest, antiresonances in a well-behaved system either always immediately precede or always immediately follow resonances.

As expected for the gaseous Sun, a modal comparison of panels a and b in Fig. 7 against Figs. 2 & 3 reveals that here extracted antiresonance modes always precede corresponding very-long-period, downwards-drifting resonance modes, as impressed onto the solar wind at its source, Fig. 7–a. This experimental confirmation of the extraction result reflects the situation in which the solar wind is a mass-driven phenomenon and not stiffness-driven, which characterizes rigid bodies. The solar wind maintains the same downward drifting and the higher order of resonances than respective antiresonances in the heliosphere as well, e.g., at the L1 point, Fig. 3–b. The data thus confirm by elimination that the here revealed resonance is the way of distributing the solar wind along very low frequencies and that (global) resonance is the natural state of that resonance, as due entirely to the Sun engine being a typical revolving-field alternator. If our Sun was not a globally structured and therefore well-behaved magnetoalternator, i.e., a real and not just a proverbial engine anymore, and if that property was not fundamental in Sun-like stars, no complete extraction of a-mode vibration could be possible from system dynamics such as the polar (fast) solar wind used here for that purpose.

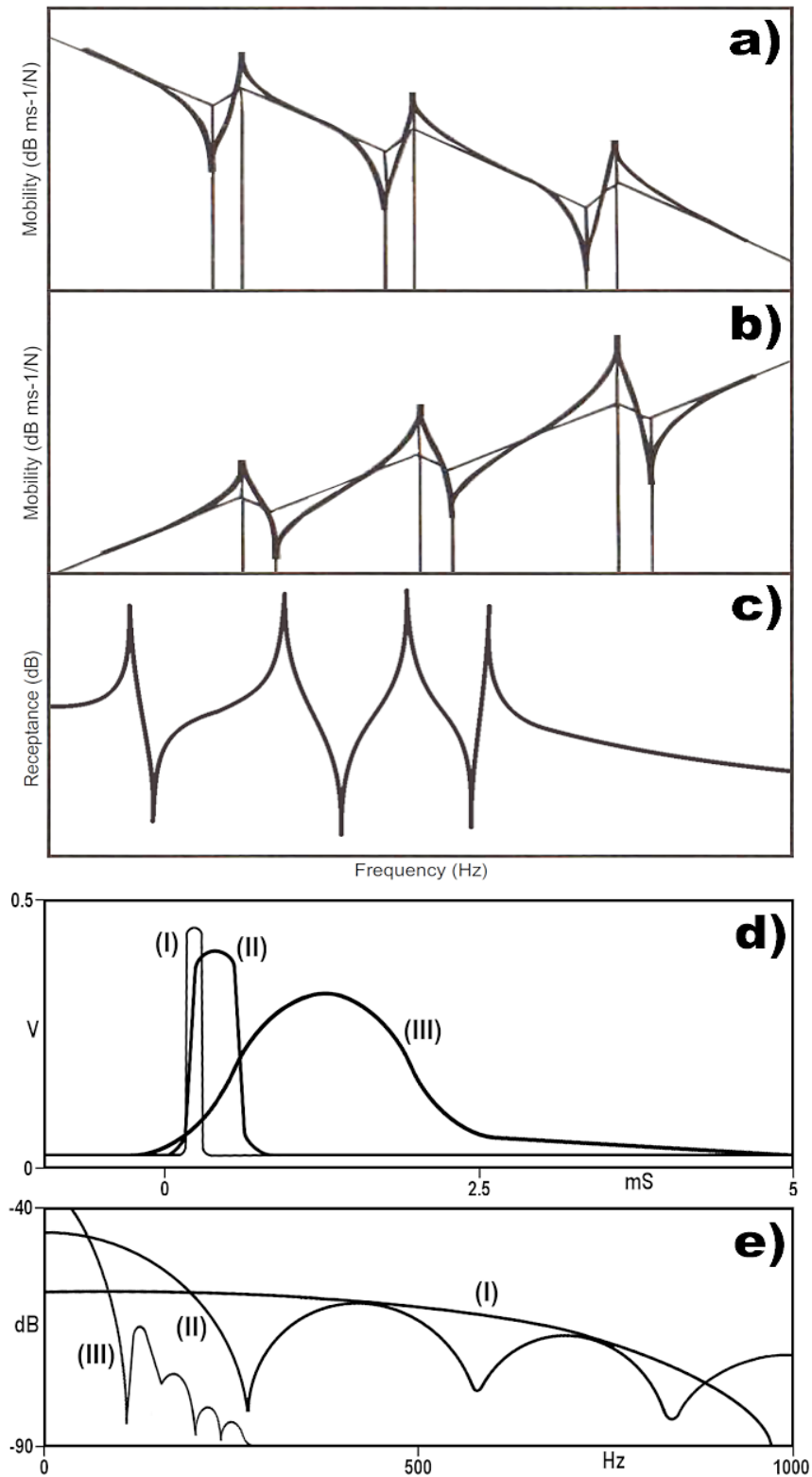


Figure 7. Panels a & b: typical dB-scaled plots of *mobility* (ratio of velocity response to force input) in a resonating body: mass-dominated mobility (panel a) that tends to drift downwards with antiresonances occurring immediately before resonances, and stiffness-dominated mobility (panel b) that generally drifts upwards and has antiresonances always immediately above resonances (Ewins, 1995). Skeleton layers represent additionally constructed ideal mass-lines and stiffness-lines, respectively, which are used in experimental studies to trace the frequency response function of resonances vs. antiresonances to examine if they are symmetric, i.e., genuine. Panel c: an example of *receptance* in a typical (resonating) damped multi-degree-of-freedom system, in dB (panel c) (He and Fu, 2001). Panels d & e: the impact type of transient excitations, from experiments with (I) an attached shaker producing the rapid sine sweep (chirp), (II) an attached shaker producing a burst — a short section of signal (random or sine) as a more general version of the rapid sine sweep, but in which the short-duration signal can take any form, and (III) a non-attached impactor such as hammer, inflicting blows upon a test structure. The response data are collected using accelerometers attached to the test structure and processed with an *analyzer* — a voltmeter-type instrument for sampling the system dynamics in volts (V) and computing a frequency response or spectrum in dB (Ewins, 1995).

Furthermore, the equal number of corresponding resonance (spectral peak-) and antiresonance (spectral trough-) periods in Fig. 3 reveals *point mobility* (force and velocity are at the same point in spectral space) rather than *transfer mobility* (at different points and thus characterized by more minima than antiresonances) of the excitation source. Furthermore, the always matching sharpness of the spectral peak–trough pairs reflects a high quality of data and analysis tools (Ewins, 1995), here the GVSA. Finally, panels d & e in Fig. 7 reveal that the signature of the Sun global resonance in the fast polar wind, Fig. 3–d & e, experimentally best matches the case II in Fig. 7–d & e. Therefore, the transient nature of solar resonances, including Rieger’s, is due to the type of alternator our Sun is, of which a specific solar cycle’s maxima and minima are then merely (apparent) stages.

5. Discussion

The traditionally favored model for the generation of Sun magnetism is that of the dynamo, a simple engine for the conversion of kinetic into electric energy that naturally gives rise to magnetism (Solanki et al., 2006). However, based on recent observations of brown dwarfs that lack a core but still exhibit the same magnetic patterns as those seen in our Sun, the mechanism could also be purely convective (Route, 2016). At the same time, based on sunspot activity observed in the past as able to shut down entirely per hemisphere, the generation mechanism could also be hemispherical (Grote and Busse, 2000). Ulysses mission, as the only ever to have scanned the Sun’s hemispheric magnetic fields in flybys over the Sun’s polar regions, has confirmed not only that magnetism in the two Sun poles differ significantly both from each other and from the equatorial magnetism but has also observed the flipping of the solar magnetism polarity every ~ 11 yr.

Heliophysics today faces two still unresolved problems of large-scale dynamics. One is **solar abundance**, i.e., a disagreement of standard stellar models (SSM) of evolution/interior for the Sun with the latest helioseismology data from the early 2000s (Bergemann and Serenelli, 2014). This discrepancy is likely due to some physical process not yet accounted for in standard solar models and could entail mixing by mechanical waves below the convection zone and down into the radiative interior and the core (Asplund et al., 2009). At the same time, although the current state of solar magnetic fields is the main indicator of the Sun’s global activity, SSMs, unfortunately, do not account for internal magnetic fields at all (Bergemann and Serenelli, 2014). The second problem is the **million-degree corona**, i.e., the overheating of the outer envelope of the Sun, to $>10^6$ °C (as opposed to a relatively much cooler photospheric/surface temperature, at $5.5 \cdot 10^3$ °C), involving millions of small-scale magnetic reconnection events of impulsive heating, called nanoflares, of up to several thousand km in size and constantly firing everywhere on the Sun (Parker, 1988).

This immense heat surplus in the corona could in theory be explained as the dissipative energy from a buildup of a large-amplitude resonance vibration of small-scale waves whenever the global wave frequency equals the local Alfvén wave frequency through the process of resonance absorption (Davila, 1987). The essential feature of that theory of the Sun and other late-type stars — under which each magnetic tube is a driven high-quality resonator — is the existence of the global mode and its subsequent coupling to the small-scale dissipative waves (ibid.). While spectra of the Sun’s p-mode (pressure-force-restoring-) and g-mode (gravity-force-restoring-) vibrations with periods of the order of 1-h or longer have been extracted entirely in heliophysics, the remaining a-mode (global; acoustically-and-magnetic-force-restoring-) vibrations spectra have not. Crude estimates indicate its periods much longer than those of the p or g modes, typically in the range of years and inexplicable by dynamo theory (Stenflo and Vogel, 1986). In addition, since the acceleration of the (fast) solar wind and the heating of the solar corona occur in essentially the same region, the underlying mechanisms of the two phenomena may be strongly linked (Grail et al., 1996) and due to the damping of Alfvén waves (Markovskii et al., 2009). This parallel is especially significant because the solar wind is a physical system characterized by multi-scale evolution; see, e.g., Verscharen et al. (2019). Since all stellar models are calibrated on the Sun and are routinely used to interpret any other star or stellar populations, completing our global knowledge of the Sun by explaining the above problems would have very large implications for our understanding of stars and galaxies in general (Bergemann and Serenelli, 2014).

Fig. 3 revealed the signature of the Sun's complete and incessant resonance in the 0.01–1.60 ZeV ($\sim 1.6 \cdot 10^7 - 2.5 \cdot 10^9$ erg) band of the solar wind's extreme (mechanical flapping) energies. This result was as expected of a magneto-alternator engine at work, with the separation of the *solar engine* (left frame) from the *Rieger resonance offshoot* subband (right frame) in which mostly macroscale phenomena of relevance for planetary geodynamics occur. While the northern wind preserves the shaking modality the best, exhibiting AR even at L1 as seen in the $\lesssim 50$ -nT 2004–2021 WIND data, the equatorially mixed (slow) wind carries only a faint AR signature. Thus the northern polar fast wind reveals its P_S global driver the most accurately and precisely, while the Rieger period in MMF turns out to be swamped by turbulence down to the 67%-significance, making P_{Rg} a feature of the northern fast wind primarily that then transmits P_{Rg} into the heliosphere. Besides, AR becomes complete (all the time preceded by companion antiresonance modes) only when the northern polar wind only is considered, Fig. 3–e. It can also be seen that the RR band begins (AR band ends) at or around the antiresonances termination frequency, which in the Sun's case turns out to be around the annual periodicity. That frequency is when the resonating system becomes decoupled but still not relaxed, and turbulences can give in to external planetary gravitation and magnetism so that, already at the lowest-frequencies-RR, the globally prominent anisotropy (seen as spectral peak splitting) yields as well. As a coupled system's energy breakdown point, the Sun's antiresonances termination at ~ 1 -yr and its $\frac{1}{2}$ harmonic are also sources of confusion, i.e., seasonal (annual and semiannual) periodicities often seen inexplicably in various records of planetary including terrestrial data, which empirically is why the 180–365-day subband is best ignored — an approach adopted in the present study as well.

As indicated in Fig. 2–d & e and confirmed in Fig. 3–d & e, AR modulates anisotropy instead of the other way around. The modulation is across all AR harmonics, so the entire Sun (characterized by anisotropy due to turbulence and overall instability of its magnetic fields) and not just some belts or layers is kept under the AR regime. As vibration magnification occurs in such close and damped vibrating systems naturally via frequency demultiplication that upsurges the energy injected resonantly into such a physical system by 100s of times (Den Hartog, 1985), we can expect a tremendous increase in dissipated heat to follow as well. For example, previously observed high-frequency (~ 12 – 42 mHz) torsional oscillations in the quiet Sun were claimed based on modeling by Srivastava et al. (2017) to be torsional Alfvén waves that transfer $\sim 10^3$ $W \cdot m^{-2}$ energy into the overlying corona, thereby heating it and facilitating the creation of the solar wind. However, those authors failed to provide an overlying mechanism for the global sustainment of such localized energy transfers, as different kinds of modeling reveal that such local transfers are insufficient to balance the Sun energy loss, e.g., by Soler et al. (2021). At the same time, the $\sim 1.6 \cdot 10^7 - 2.5 \cdot 10^9$ erg base energies of the global mechanism found herein can multiply $\sim 10^2$ -fold or more via the said frequency demultiplication and thereby supply the minimum input energy required to balance the chromosphere's and corona's losses to radiation and supersonic wind, of $\sim 10^2 - 10^4$ $W \cdot m^{-2}$ (Withbroe and Noyes, 1977). All these characteristics of how resonance–antiresonance (constructive vs. destructive waves) couplings dominate turbulence help discern the northern and southern fast wind as the original (released as intended) winds, i.e., the most faithful representation of the Sun internal engine at work. The polar (fast) winds thus overall reflect the operational regime of the Sun under which it emits them. Note here that, amongst all characteristic data sets examined, statistical fidelity favors the northern polar fast wind most of the time, Fig. 5.

The above-discussed moderation of anisotropy by AR is not the only reformatting on global scales. Thus as seen in Fig. 3-b, besides signal purity breaking down temporally beyond/above the antiresonance train's termination point at ~ 1 -yr periodicity when the global coupling ceases, the Sun vibration does not relax either. It also breaks down spatially beyond L1, leaving RR open to external influences such as planetary constellations and fields, gravitational and magnetic primarily. Such interplay has been suggested previously, e.g., by Kurochkin (1998) and Abreu et al. (2012), who proposed such gravitational and orbital-resonance effects on the Rieger process. Earlier, Pap et al. (1990) had offered an intuitive explanation that the existence of a transient 154 ± 13 -day (Rieger) period was related to an emerging strong magnetic field. As can be seen from Fig. 3, after decades of debates, P_{Rg} turned out to be a genuine Sun period that experiences modulations in the heliosphere, while most if not all Rieger-type and longer periodicities as modified externally have been reported in various types of data in heliophysics; see, e.g., Forgacs-Dajka and Borkovits (2007). The secret to the Rieger period's strength as well as stability and presence in most solar indices lies in it being globally (as sensed here in both the northern and southern polar winds) the tailing $\geq 99\%$ -significant harmonic of the Sun antiresonance twice (N and S simultaneously). While all those

reports were demonstrably correct, Fig. 3 and Table 1, planetary fields can reformat the Rieger harmonics, somewhat disturbing the widely reported values listed in Introduction, as seen from the steadiness of $\frac{1}{2}P_{Rg}$ as the one they do not, Fig. 5–callout. As mentioned, these disturbances primarily come from the most dominant gravitational and magnetic fields in the solar system. Besides, global resonances in closed spherical systems can arise externally and internally. However, in stars with a non-uniform rotation like our Sun, no external triggering is possible, and a continuous spectrum of modes can be expected that can undergo amplification when subjected to a disturbing force of the appropriate frequency, and hence lead to enhanced dissipation (Papaloizou and Pringle, 1978). But even in the opposite case, the main external factors would be closely related to variations in orbital parameters; however, the Sun’s most relevant such parameters — precession and obliquity — are related practically entirely to Jupiter gravitational influence and can be safely ruled out since creating a negligible effect which on the Sun amount to under 1 mm.

Thus the primary candidate for the AR triggering mechanism is couplings amongst the normal modes of vibration of latitudinally varied belts of the Sun, here extracted as ~ 11 -, ~ 10 -, and ~ 9 -yr; see, e.g., Cole (2008). More precisely, these varying but mutually superimposed global modes as found in the present study are 9.9-yr for both MMF (by WSO) and N–S polar fields combined (by Ulysses), 11.2-yr both for the IMF at L1 (by WIND) and the IMF above the northern region (by Ulysses), and 8.8-yr for the southern field (by Ulysses), Fig. 3. The Sun–Heliosphere congruency in periods of the AR lead modes is as expected from a global resonance propagated to L1 and beyond. These excellent matches from data sets that are significantly disparate in length, density, field strength, and sampled epoch reflect the northern polar fast wind dominance of the heliosphere as far as $\sim L1$ distances. The matchings also reveal both clarity of the signal and GVSA superiority over the Lomb-Scargle and wavelets spectral techniques as applied by Stenflo and Vogel (1986) and Knaack and Stenflo (2005) for their claimed partial recovery of r- and R-mode fragments of the continuous a-mode global resonance.

The discovery that the solar wind gets emitted in the form of a very-low-frequency mechanical resonance, which is maintained as far as L1, is good news for the Earth since this find enables more concentrated efforts at modeling the wind impact on Earth. In addition, as found for the solar cycles examined herein, the isolating of the northern polar wind as the physically most vigorous pusher of solar ejecta has important implications for modeling solar-terrestrial interactions and forecasting space weather.

The here-presented spectral study of the $B < 30 \mu T$ IMF in the solar wind at the wind’s presumed sources investigated the wind’s global dynamics in the 1-mo-1-yr band. For this purpose, the wind was separated in its slow, predominantly equatorial component, represented in the above band of global resonance by MMF observations from the WSO telescope, and the fast component, emitted by the polar fields and observed by the Ulysses spacecraft magnetometer and also represented by PF data from the WSO telescope. Since decadal samplings of the near solar wind spanning around one Hale cycle or two $P_s = \sim 11$ -yr (Schwabe) cycles are now available for the same interplanetary sector, at L1, those magnetometer measurements from the WIND mission also were used to verify the result. The multi-mission comparison of solar wind and its components’ sources revealed with $\geq 99\%$ confidence that the Sun northern polar region drives the fast wind at P_s , with the slow solar wind emitted or mixed equatorially, at the P_s degenerated into a ~ 10 -yr global mode, Fig. 3–a. The difference triggers a perfect (integer-ordered) 3D mechanical resonance in the wind’s waving at least up to degree $m=131$. Due to turbulent and wandering local fields, the Sun southern polar region emits the solar wind along a P_s degenerated into a ~ 9 -yr global mode and under progressive anisotropy towards lower frequencies so that P_s harmonics get recovered completely. Thus, of all known magnetism-related solar periods, the ~ 11 -yr Schwabe cycle is the guide period, while longer periodicities reflect the differentially triggered resonance so that the longest, ~ 88 -yr Gleissberg, such period is a superimposition reflection of the 11–10–9 coupling. Acting globally as an asymmetrically vibrating (and therefore resonating) magnetic alternator, the Sun fully exerts control over the entire heliosphere domain, i.e., of both solar wind’s resonances (near winds) and turbulences (near and far winds). This successful spectral separation of very-low-frequency (down to P_s) slow v. fast solar wind via extraction of their unique but comparable spectral signatures paves the way for global and differential studies of heliosphere using AR and generally for all future modeling of local stellar wind and planetary geodynamics. Heliosphere’s hypothetical magnetic structure, believed to be composed of random flux tubes, is herein superseded by a centrally and virtually completely guided mechanical resonance of the alternating fast-slow solar wind blanketing and flapping resonantly-quasiperiodically about the ecliptic.

As found by Stenflo and Vogel (1986) in their partial recovery of AR from Sun data, the global magnetic field has a patterned (modal) structure characterized by sharp global resonances decoupled from each other for the modes of odd and even parity, thus indicating the existence of an underlying selection rule. While failing to extract the complete AR information, including antiresonances and the Rieger resonance, those authors concluded that this new emission-line spectrum of solar magnetic fields does not seem to be explicable within the framework of current concepts such as dynamo theory but should contain potentially powerful diagnostic information on the interior magnetic structure of the Sun and the origins of solar activity. Their conclusion agrees with what was arrived at herein, Figs. 2-4 and Tables 1-3, after various crosschecks including an agreement with experiment, Fig. 7, examination of resonance preservation at L1, Fig. 3-b, and verification against WSO polar-field data, Fig. 6.

Thus as a star with a differentially rotating core (Fossat et al., 2017), the Sun as a whole is a (globally) self-resonating ring-system of belts and layers that both contrarily vibrate and differentially rotate, and in which therefore no particular layer or field (toroidal or spheroidal, i.e., poloidal), is singly responsible for the a-mode global resonance. This mechanism, which is not strictly Alfvén resonance but involves both the Alfvén waves and the shear mode, is easily extended to the normal stars class of our Sun. On the other hand, the more massive stars beyond the Sun class were, based on theoretical modeling, speculated previously to release their stellar wind due to radiation pressure on the stellar atmospheric dust, e.g., by Mattsson et al. (2010). However, disentangling the various feedback mechanisms in massive stars, including stellar wind, only becomes possible with observations spanning a significant range of environments, as this allows to probe dependences on metallicity, size, stellar, and dust contents (McLeod et al., 2019).

Based on the herein presented results in the dynamic energy ranges, the (northern) polar solar wind appears to be the 'main' or 'normal' solar wind in the solar cycle examined in the present study. Heliosphere's hypothetical magnetic structure imagined by some to be composed of turbulently random flux tubes or ropes is superseded by a guided resonating flux of alternating fast-slow jets blanketing and flapping quasiperiodically (locally transiently) about the ecliptic..

6. Conclusions

The inner workings of the Sun as a classical revolving-field magnetoalternator and not just proverbial engine anymore were extracted herein for the first time and to an unprecedented (absolute) accuracy and precision, from the Ulysses mission scans of the interplanetary magnetic field above the Sun northern and, separately, southern polar regions. The virtually complete extraction means that the solar wind is being generated at highly coherent, discrete wave modes in the Sun, which get effortlessly transported to distances beyond L1. The rigorous Gauss–Vaniček spectral analysis method, based on strict least-squares fitting and statistical and physical criteria for the significance of spectral contents, was used to extract the complete and incessant global resonance of the Sun as imprinted in the polar (fast) solar winds. With its unique statistical-physical rigor, this method has turned out to be superior by far to any Fourier, approximate least-squares fitting like the Lomb-Scargle, or wavelets techniques used in the past to claim (partial) extractions of Sun global resonances.

Spectral analysis of separated northern and southern polar (fast) solar wind, both taken to be the original solar wind where the former recreates Sun resonances more faithfully, has thus revealed the signature of a Sun as a real magnetic alternator engine that naturally both vibrates and resonates, resembling the theoretical concept of *Alfvén resonance*. The data further showed that, as with any mechanical resonance, the Sun global resonance too is far more complex, preceded by antiresonances, and does not lend itself to theoretical simplifications, so empirical considerations were invoked, showing that the result also agrees with experimental evidence in addition to an agreement with disparate data. The Sun engine is a ring system of separately vibrating and rotating conveyor belts, with an added complexity of differentially rotating, contrarily (out-of-phase) vibrating, and vertically stratified layers. Because of this, while working in unison with solar cycles as the common-denominator pulsation driver that periodically emerges from all the mutually struggling possibilities within the frequency space, the Sun then releases the solar wind as a result of structural instability, in a shake-off similar to that of a motor engine trying to rid itself of its casing

while experiencing a global mechanical resonance itself. The data further showed that gravitation could couple spontaneously with the ~150–160-day Rieger period mode, known to dominate planetary geodynamics, resulting in the well-known Rieger-type periodicities (Rieger resonance) whose existence demonstrates the viability of gravitomagnetics on star-system scales. The Rieger period arises as the offshoot of the global Alfvén resonance at the antiresonance-termination (couplings-cessation) point, whose double-power (stemming from simultaneous emission from both northern and southern polar regions) gets channeled through the heliosphere unobstructed and forms a gravitomagnetically modified Rieger resonance — physical waves of flapping solar ejecta pushed outwards and thereby sped up. The Rieger period gets its value of ~154 days from being the triple (tri-band) resonance response of the Sun to its three significantly contrary (out-of-phase) global vibrations (~11, ~10, ~9-yr) around the global mode, i.e., $P_{Rg}=P_S/3/3/3$.

While the concept of a global magnetoalternator engine is readily extendable to normal-type stars like our Sun, this concept of the solar wind as simply the Sun’s resonant shake-off is probably extendable not only to the stellar wind as such but to planetary atmospheric winds and Earth mantle wind as well. Thermally differentiated masses are stirred mechanically-resonantly in an attempt of the host body to equilibrate by ridding itself as quickly as possible of the “weakest link” — the topmost least dense layer alongside the contact interface with the next (~zero-density) layer radially outwards (above). Within its energy budget that includes resonantly magnified energies, the same then mechanism allows for the solar abundance and million-degree corona phenomena. This discovery, accompanied by the first complete extraction of the global Alfvén resonance from *in situ* data and the deciphering of the origin of the Rieger period and Rieger-type periodicities that play a crucial role throughout the Solar system’s dynamics, pave the way for detailed studies of the Sun and heliosphere, as well as for a new fundamental understanding of a myriad of other stars and stellar systems.

Acknowledgments

The least-squares spectral analysis scientific software LSSA, based on the rigorous method by Vaníček (1969, 1971), was used to compute spectra. Dr. Spiros Pagiatakis (York University) provided LSSA v.5.0, which is now available as an open-source version from <http://www2.unb.ca/gge/Research/GRL/LSSA/sourceCode.html>.

Data sources

WIND data are from https://wind.nasa.gov/data_sources.php#MFI_Data. WSO MMF data are from <http://wso.stanford.edu/#MeanField>. WSO PF data are from <http://wso.stanford.edu/Polar.html>. Ulysses data are from the National Space Science Data Center, Principal Investigator A. Balogh, Imperial College, London, UK: <https://spdf.gsfc.nasa.gov/pub/data/ulysses/mag/interplanetary/hour/>. All data analyzed are enclosed in a Supplement accompanying this manuscript.

Declarations

The author declares no competing interests.

References

- Abreu, J.A., Beer, J., Ferriz-Mas, A., McCracken, K.G., Steinhilber, F. (2012) Is there a planetary influence on solar activity? *Astron. Astroph.* 548:A88. DOI: <https://doi.org/10.1051/0004-6361/201219997>
- Alfvén, H. (1943) On Sunspots and the Solar Cycle. *Arkiv f. Mat., Astron. o. Fys.* 29A(12):1–17. BIB: <https://ui.adsabs.harvard.edu/abs/1943ArMAF..29R...1A>
- Alfvén, H. (1942) Existence of electromagnetic-hydrodynamic waves. *Nature* 150(3805):405–406. DOI: <https://doi.org/10.1038%2F150405d0>
- Alfvén, H. (1948) *Cosmical electrodynamics*. Oxford University Press (2nd ed. Clarendon Press, 1963), 228 pp. ISBN 9780198512011
- Asplund, M., Grevesse, N., Sauval, A.J., Scott, P. (2009) The chemical composition of the Sun. *Ann. Rev. Astron. Astrophys.* 47(1):481–522. DOI: <https://doi.org/10.1146/annurev.astro.46.060407.145222>
- Bai T. and Cliver E. W. (1990) A 154 day periodicity in the occurrence rate of proton flares. *Astrophys. J.* 363:299–309. DOI: <https://doi.org/10.1086/169342>
- Bellan, P.M. (1996) Mode conversion into non-MHD waves at the Alfvén layer: The case against the field line resonance concept. *J. Geophys. Res.* 101(A11):24887–24898. DOI: <https://doi.org/10.1029/96JA02253>
- Bellan, P.M. (1994) Alfvén ‘resonance’ reconsidered: Exact equations for wave propagation across a cold inhomogeneous plasma. *Phys. Plasmas* 1:3523–3541. DOI: <https://doi.org/10.1063/1.870888>
- Bergemann M., Serenelli A. (2014) Solar Abundance Problem. In: Niemczura E., Smalley B., Pych W. (Eds.) *Determination of Atmospheric Parameters of B-, A-, F- and G-Type Stars. GeoPlanet: Earth and Planetary Sciences*. Springer, Cham. DOI: https://doi.org/10.1007/978-3-319-06956-2_21
- Borovsky, J.E. (2018) The spatial structure of the oncoming solar wind at Earth and the shortcomings of a solar-wind monitor at L1. *J. Atmo. Solar-Terr. Phys.* 177:2-11. DOI: <https://doi.org/10.1016/j.jastp.2017.03.014>
- Bose, S., Nagaraju, K. (2018) On the variability of the Solar Mean Magnetic Field: contributions from various magnetic features on the surface of the Sun. *Astrophys. J.* 862:35. DOI: <https://doi.org/10.3847/1538-4357/aaccf1>
- Brooks, D., Ugarte-Urra, I., Warren, H. (2015) Full-Sun observations for identifying the source of the slow solar wind. *Nat. Commun.* 6:5947. DOI: <https://doi.org/10.1038/ncomms6947>
- Bruno, R., Carbone, V. (2013) The solar wind as a turbulence laboratory. *Living Rev. Sol. Phys.* 10:2. DOI: <https://doi.org/10.12942/lrsp-2013-2>
- Campos, L. (1977) On the generation and radiation of magneto-acoustic waves. *J. Fluid Mech.* 81(3):529–549. DOI: <https://doi.org/10.1017/S0022112077002213>
- Cane, H.V., Richardson, I.G., von Rosenvinge, T.T. (1998) Interplanetary magnetic field periodicity of ~153 days. *Geophys. Res. Lett.* 25(24):4437–4440. DOI: <https://doi.org/10.1029/1998GL900208>
- Carbonell, M., Oliver, R., Ballester, J.L. (1992) Power spectra of gapped time series: a comparison of several methods. *Astron. & Astrophys.* 264:350–360. BIB: <https://ui.adsabs.harvard.edu/#abs/1992A&A...264..350C>
- Choi, K.-E., Lee, D.-Y. (2019) Origin of solar rotational periodicity and harmonics identified in the Interplanetary Magnetic Field B_z component near the Earth during solar cycles 23 and 24. *Sol. Phys.* 294:44. DOI: <https://doi.org/10.1007/s11207-019-1433-7>
- Cole, M.O.T (2008) On stability of rotordynamic systems with rotor–stator contact interaction. *Proc. R. Soc. A.* 4643353–3375. DOI: <https://doi.org/10.1098/rspa.2008.0237>
- Daničević, S., Vince, I., Vitas, N., Jovanović, P. (2005) Time series analysis of long term full disk observations of the Mn I 539.4 nm solar line. *Serb. Astron. J.* 170:79–88. DOI: <https://doi.org/10.2298/SAJ0570079D>
- Davila, J.M. (1987) Heating of the solar corona by the resonant absorption of Alfvén waves. *Astrophys. J.* 317:514–521. BIB: <https://ui.adsabs.harvard.edu/#abs/1987ApJ...317..514D>
- Den Hartog, J.P. (1985) *Mechanical Vibrations*. Dover Publications, New York, United States. ISBN 0486647854
- Deng, L.H. Li, B., Xiang, Y.Y., Dun, G.T. (2014) On mid-term periodicities of high-latitude solar activity. *Adv. Space Res.* 54(1):125–131. DOI: <https://doi.org/10.1016/j.asr.2014.03.006>
- Deubner, F.-L., Gough, D. (1984) Helioseismology: Oscillations as a Diagnostic of the Solar Interior. *Ann. Rev. Astron. Astrophys.* 22(1):593–619. DOI: <https://doi.org/10.1146/annurev.aa.22.090184.003113>
- Dimitropoulou, M., Moussas, X., Strintzi, D. (2008) Enhanced Rieger type periodicities' detection in X-ray solar flares and statistical validation of Rossby waves' existence. *Proc. Int. Astron. Union* 4(S257):159–163. DOI: <https://doi.org/10.1017/S1743921309029226>
- Dzhalilov, N.S., Staude, J., Oraevsky, V.N. (2002) Eigenoscillations of the differentially rotating Sun - I. 22-year, 4000-year, and quasi-biennial modes. *Astron. Astrophys.* 384(1):282–298. DOI: <https://doi.org/10.1051/0004-6361:20011836>

- Ewins, D.J. (1995) *Modal Testing: Theory and Practice*. Research Studies Press Ltd., Taunton, England, ISBN 0863800173. John Wiley & Sons Inc., ISBN 04719904724. 313 pp.
- Forgacs-Dajka, E., Borkovits, T. (2007) Searching for mid-term variations in different aspects of solar activity – looking for probable common origins and studying temporal variations of magnetic polarities. *Mon. Not. R. Astron. Soc.* 374:282–291. DOI: <https://doi.org/doi:10.1111/j.1365-2966.2006.11167.x>
- Fossat, E., Boumier, P., Corbard, T., Provost, J., Salabert, D., Schmider, F.X., Gabriel, A.H., Grec, G., Renaud, C., Robillot, J.M., Roca-Cortés, T., Turck-Chièze, S., Ulrich, R.K., Lazrek, M. (2017) Asymptotic g modes: Evidence for a rapid rotation of the solar core. *Astron. Astrophys.* 604:A40. DOI: <https://doi.org/10.1051/0004-6361/201730460>
- Goedbloed, J.P., Lifschitz, A. (1995) Comment on "Alfvén 'resonance' reconsidered: Exact equations for wave propagation across a cold inhomogeneous plasma" [Phys. Plasmas 1:3523 (1994)]. *Phys. Plasmas* 2:3550–3551. DOI: <https://doi.org/10.1063/1.871471>
- Gough, D. (1995) Waves in the wind. *Nature* 376:120–121. DOI: <https://doi.org/10.1038/376120a0>
- Grail, R., Coles, W., Klinglesmith, M., Breen, A.R., Williams, P.J.S., Markkanen, J., Esser, R. (1996) Rapid acceleration of the polar solar wind. *Nature* 379:429–432. DOI: <https://doi.org/10.1038/379429a0>
- Grant, S.D.T., Jess, D.B., Zaqarashvili, T.V. Beck, C., Socas-Navarro, H., Aschwanden, M.J., Keys, P.H., Christian, D.J., Houston, S.J., Hewitt, R.L. (2018) Alfvén wave dissipation in the solar chromosphere. *Nature Phys.* 14:480–483. DOI: <https://doi.org/10.1038/s41567-018-0058-3>
- Grote, E., Busse, F.H. (2000) Hemispherical dynamos generated by convection in rotating spherical shells. *Phys. Rev. E* 62:4457–4460. DOI: <https://doi.org/10.1103/PhysRevE.62.4457>
- Gurgenashvili, E., Zaqarashvili, T.V., Kukhianidze, V., Oliver, R., Ballester, J.L., Dikpati, M., McIntosh, S.W. (2017) North–South Asymmetry in Rieger-type Periodicity during Solar Cycles 19–23. *Astrophys. J.* 845(2):137–148. DOI: <https://dx.doi.org/10.3847/1538-4357/aa830a>
- Gurgenashvili, E., Zaqarashvili, T.V., Kukhianidze, V., Oliver, R., Ballester, J.L., Ramishvili, G., Shergelashvili, B., Hanslmeier, A., Poedts, S. (2016) Rieger-type periodicity during solar cycles 14–24: estimation of dynamo magnetic field strength in the solar interior. *Astrophys. J.* 826(1):55. DOI: <https://doi.org/10.3847/0004-637X/826/1/55>
- He, J., Fu, Z.-F. (2001) *Modal Analysis*. Butterworth-Heinemann. ISBN 9780750650793. DOI: <https://doi.org/10.1016/B978-0-7506-5079-3.X5000-1>
- Jones, G., Balogh, A. (2003) The global heliospheric magnetic field polarity distribution as seen at Ulysses. *Annales Geophysicae* 21(6):1377–1382. DOI: <https://doi.org/10.5194/angeo-21-1377-2003>
- Kasper, J.C., Maruca, B.A., Stevens, M.L., Zaslavsky, A. (2013) Sensitive Test for Ion-Cyclotron Resonant Heating in the Solar Wind. *Phys. Rev. Lett.* 110:091102. DOI: <https://doi.org/10.1103/PhysRevLett.110.091102>
- Kinkhabwala, A. (2013) *Maximum Fidelity*. Max Planck Institute of Molecular Physiology report. arXiv: <https://arxiv.org/abs/1301.5186>
- Knaack, R., Stenflo, J.O. (2005) Spherical harmonic decomposition of solar magnetic fields. *Astron. Astrophys.* 438(1):349–363. DOI: <https://doi.org/10.1051/0004-6361:20052765>
- Kurochkin, N.E. (1998) Transient periodicity in solar activity. *Astron. Astrophys. Trans.* 15(1–4):277–279. DOI: <https://doi.org/10.1080/10556799808201781>
- Markovskii, S.A., Vasquez, B.J., Hollweg, J.V. (2009) Proton heating by nonlinear field-aligned Alfvén waves in solar coronal holes. *Astrophys. J.* 695(2):1413. DOI: <https://doi.org/10.1088/0004-637X/695/2/1413>
- Mattsson, L., Wahlin, R., Höfner, S. (2010) Dust driven mass loss from carbon stars as a function of stellar parameters - I. A grid of solar-metallicity wind models. *Astron. Astrophys.* 509:A14. DOI: <https://doi.org/10.1051/0004-6361/200912084>
- McLeod, A.F., Dale, J.E., Evans, C.J., Ginsburg, A., Kruijssen, J.M.D., Pellegrini, E.W., Ramsay, S.K., Testi, L. (2019) Feedback from massive stars at low metallicities: MUSE observations of N44 and N180 in the Large Magellanic Cloud. *Mon. Not. R. Astron. Soc.* 486:5263–5288. DOI: <https://doi.org/10.1093/mnras/sty2696>
- Omerbashich, M. (2021a) Non-marine tetrapod extinctions solve extinction periodicity mystery. *Hist. Biol.* 34 (29 March). DOI: <https://doi.org/10.1080/08912963.2021.1907367>
- Omerbashich, M. (2007) Erratum due to journal error. *Comp. Sci. Eng.* 9(4):5–6. DOI: <https://doi.org/10.1109/MCSE.2007.79>; full text: <https://arxiv.org/abs/math-ph/0608014>
- Omerbashich, M. (2006) Gauss–Vaníček Spectral Analysis of the Sepkoski Compendium: No New Life Cycles. *Comp. Sci. Eng.* 8(4):26–30. DOI: <https://doi.org/10.1109/MCSE.2006.68>
- Omerbashich, M. (2003) *Earth-model Discrimination Method*. Ph.D. Dissertation, pp.129. ProQuest, USA. DOI: <https://doi.org/10.6084/m9.figshare.12847304>
- Pagiatakis, S. (1999) Stochastic significance of peaks in the least-squares spectrum. *J. Geod.* 73:67–78. DOI: <https://doi.org/10.1007/s001900050220>

- Pap, J., Tobiska, W.K., Bouwer, S.D. (1990) Periodicities of solar irradiance and solar activity indices, I. *Sol. Phys.* 129:165–189. DOI: <https://doi.org/10.1007/BF00154372>
- Papaloizou, J., Pringle, J.E. (1978) Non-radial oscillations of rotating stars and their relevance to the short-period oscillations of cataclysmic variables. *Mon. Not. R. Astron. Soc.* 182:423–442. DOI: <https://doi.org/10.1093/mnras/182.3.423>
- Parker, E.N. (1988) Nanoflares and the solar X-ray corona. *Astrophys. J.* 330:474–479. BIB: <https://ui.adsabs.harvard.edu/abs/1988ApJ...330..474P>
- Press, W.H., Teukolsky, S.A., Vetterling, W.T., Flannery, B.P. (2007) *Numerical Recipes: The Art of Scientific Computing* (3rd Ed.). Cambridge University Press, United Kingdom. ISBN 9780521880688
- Rieger, E., Share, G.H., Forrest, D.J., Kanbach, G., Reppin, C., Chupp, E.L. (1984) A 154-day periodicity in the occurrence of hard solar flares? *Nature* 312:623–625. DOI: <https://doi.org/10.1038/312623a0>
- Robson J.D., Dodds C.J., Macvean D.B., Paling, V.R. (1971) Vibration Theory I: Receptance. In: *Random Vibrations*. International Centre for Mechanical Sciences (Courses and Lectures), Vol. 115. Springer, Vienna. DOI: https://doi.org/10.1007/978-3-7091-2734-6_4
- Route, M. (2016) The discovery of solar-like activity cycles beyond the end of the main sequence? *Astrophys. J. Lett.* 830:L27. DOI: <https://doi.org/10.3847/2041-8205/830/2/L27>
- Scherrer, P.H., Wilcox, J.M., Svalgaard, L., Duvall, Jr. T.L., Dittmer, P.H., Gustafson, E.K. (1977) The mean magnetic field of the Sun: Observations at Stanford. *Sol. Phys.* 54:353–361. DOI: <https://doi.org/10.1007/BF00159925>
- Schwabe, H. (1844) Solar observations during 1843. *Astronomische Nachrichten* 20(495):233–236. BIB: <https://ui.adsabs.harvard.edu/abs/1844AN.....21..233S>
- Shannon, C.E. (1948) A Mathematical Theory of Communication. *Bell System Tech. J.* 27:379–423, 623–656. DOI: <https://doi.org/10.1002/j.1538-7305.1948.tb01338.x>
- Singh, Y.P., Badruddin (2019) Study of the solar rotational period and its harmonics in solar activity, interplanetary, geomagnetic, and cosmic ray intensity indicators during solar polarity reversal periods. *Sol. Phys.* 294:27. DOI: <https://doi.org/10.1007/s11207-019-1413-y>
- Smith, E.J., Marsden, R.G. (2003) Ulysses observations at solar maximum: introduction. *Geophys. Res. Lett.* 30:8027. DOI: <https://doi.org/10.1029/2003GL018223>
- Solanki, S.K., Inhester, B., Schussler, M. (2006) The solar magnetic field. *Rep. Prog. Phys.* 69(3):563–668. DOI: <https://doi.org/10.1088/0034-4885/69/3/R02>
- Soler, R., Terradas, J., Oliver, R., Ballester, J.L. (2021) Resonances in a coronal loop driven by torsional Alfvén waves propagating from the photosphere. *Astrophys. J.* 909(2):190. DOI: <https://doi.org/10.3847/1538-4357/abdec5>
- Sorriso-Valvo, L., Marino, R., Carbone, V., Noullez, A., Lepreti, F., Veltri, P., Bruno, R., Bavassano, B., Pietropaolo, E. (2007) Observation of Inertial Energy Cascade in Interplanetary Space Plasma. *Phys. Rev. Lett.* 99(11):115001. DOI: <https://doi.org/10.1103/PhysRevLett.99.115001>
- Steeves, R.R. (1981). *A statistical test for significance of peaks in the least squares spectrum*. Collected Papers, Geodetic Survey, Department of Energy, Mines and Resources. Surveys and Mapping Branch, Ottawa Canada, pp. 149–166.
- Srivastava, A., Shetye, J., Murawski, K., Doyle, J.G., Stangalini, M., Scullion, E., Ray, T., Wojcik, D.P., Dwivedi, B.N. (2017) High-frequency torsional Alfvén waves as an energy source for coronal heating. *Sci. Rep.* 7:43147. DOI: <https://doi.org/10.1038/srep43147>
- Stenflo, J., Vogel, M. (1986) Global resonances in the evolution of solar magnetic fields. *Nature* 319:285–290. DOI: <https://doi.org/10.1038/319285a0>
- Taylor, J., Hamilton, S. (1972) Some tests of the Vaníček Method of spectral analysis. *Astrophys. Space Sci.* 17:357–367. DOI: <https://doi.org/10.1007/BF00642907>
- Thomas, S.R., Owens, M.J., Lockwood, M. (2014) The 22-year Hale Cycle in cosmic ray flux: evidence for direct heliospheric modulation. *Sol. Phys.* 289(1):407–421. DOI: <https://doi.org/10.1007/s11207-013-0341-5>
- Thomson, D., MacLennan, C., Lanzerotti, L. (1995) Propagation of solar oscillations through the interplanetary medium. *Nature* 376:139–144. DOI: <https://doi.org/10.1038/376139a0>
- Tokumar, M., Fujiki, K., Iju, T. (2015) North-south asymmetry in global distribution of the solar wind speed during 1985–2013. *J. Geophys. Res. Space Phys.* 120:3283–3296. DOI: <https://doi.org/10.1002/2014JA020765>
- Vaniček, P. (1969) Approximate spectral analysis by least-squares fit. *Astrophys. Space Sci.* 4(4):387–391. DOI: <https://doi.org/10.1007/BF00651344>
- Vaniček, P. (1971) Further development and properties of the spectral analysis by least-squares fit. *Astrophys. Space Sci.* 12(1):10–33. DOI: <https://doi.org/10.1007/BF00656134>
- Vecchio, A., Carbone, V. (2009) Spatio-temporal analysis of solar activity: main periodicities and period length variations. *Astron. Astrophys.* 502(3):981–987. DOI: <https://doi.org/10.1051/0004-6361/200811024>

Verscharen, D., Klein, K.G., Maruca, B.A. (2019) The multi-scale nature of the solar wind. *Living Rev. Sol. Phys.* 16:5, pp.136. DOI: <https://doi.org/10.1007/s41116-019-0021-0>

Wells, D.E., Vaníček, P., Pagiatakis, S. (1985) *Least squares spectral analysis revisited*. Department of Geodesy & Geomatics Engineering Technical Report 84, University of New Brunswick, Canada. URL: <http://www2.unb.ca/gge/Pubs/TR84.pdf>

Withbroe, G.L., Noyes, R.W. (1977) Mass and Energy Flow in the Solar Chromosphere and Corona. *Ann. Rev. Astron. Astrophys.* 15(1):363–387. DOI: <https://doi.org/10.1146/annurev.aa.15.090177.002051>

Wolff, C.L., Blizard, J.B. (1986) Properties of r-modes in the Sun. *Sol. Phys.* 105:1–15. DOI: <https://doi.org/10.1007/BF00156371>

Zaqarashvili, T.V., Carbonell, M., Oliver, R., Ballester, J.L. (2010) Magnetic Rossby waves in the solar tachocline and Rieger-type periodicities. *Astrophys. J.* 709(2):749–758. DOI: <https://doi.org/10.1088/0004-637X/709/2/749>